Loss of epithelial G_q and G_{11} signaling inhibits TGFβ production but promotes IL-33–mediated macrophage polarization and emphysema

Alison E. John,[1*] Michael. R. Wilson, [2] Anthony Habgood,[1] Joanne Porte,[1] Amanda L. Tatler,[1] Anastasios Stavrou,[1] Gino Miele,[3] Lisa Jolly,[1] Alan J. Knox,[1] Masao Takata,[2] Stefan Offermanns,[4] R. Gisli Jenkins[1]

[1]Respiratory Medicine, University of Nottingham, Nottingham, UK. [2]Anaesthetics, Pain Medicine and Intensive Care, Imperial College, London, UK. [3]Epistem Ltd, Manchester, UK. [4]Department of Pharmacology, Max-Planck-Institute for Heart and Lung Research, Bad Nauheim, Germany.

[*]Corresponding author. Email: alison.john@nottingham.ac.uk

Abstract

Heterotrimeric guanine nucleotide–binding protein (G protein) signaling links hundreds of G protein–coupled receptors (GPCRs) with four G protein signaling pathways. Two of these, one mediated by G_q and G_{11} ($G_{q/11}$) and the other by G_{12} and G_{13} ($G_{12/13}$), are implicated in the force-dependent activation of transforming growth factor–β (TGFβ) in lung epithelial cells. Reduced TGFβ activation in alveolar cells leads to emphysema, whereas enhanced TGFβ activation promotes acute lung injury and idiopathic pulmonary fibrosis. Therefore, precise control of alveolar TGFβ activation is essential for alveolar homeostasis. Here, we investigated the involvement of the $G_{q/11}$and $G_{12/13}$ pathways in epithelial cells in generating active TGFβ and regulating alveolar inflammation. Mice deficient in both $G\alpha_q$ and $G\alpha_{11}$ developed inflammation that was primarily caused by alternatively activated (M2-polarized) macrophages, enhanced matrix metalloprotease 12 (MMP12) production, and age-related alveolar airspace enlargement consistent with emphysema. Mice with impaired $G_{q/11}$ signaling had reduced stretch-mediated generation of TGFβ by epithelial cells and enhanced macrophage MMP12 synthesis, but were protected from the effects of ventilator-induced lung injury. Furthermore, synthesis of the cytokine interleukin-33 (IL-33) was increased in these alveolar epithelial cells, resulting in the M2-type polarization of alveolar macrophages

independently of the effect on TGFβ. Our results suggest that alveolar $G_{q/11}$ signaling maintains alveolar homeostasis, and likely independently increases TGFβ activation in response to mechanical stress of the epithelium and decreases epithelial IL-33 synthesis. Together, these findings suggest that disruption of $G_{q/11}$ signaling promotes inflammatory emphysema but protects against mechanically induced lung injury.

Introduction

Heterotrimeric guanine nucleotide–binding protein (G protein) signaling is a ubiquitous system that couples many hundreds of G protein–coupled receptors (GPCRs) to a diverse array of effector molecules. Despite the huge diversity of receptors and effectors, there are only four families of heterotrimeric G proteins: G_S, Gi/Go, Gq/G11, and G12/G13. Two of these families (Gq/G11 and G12/G13) mediate activation of the RhoA signaling pathways (1, 2). Work by our group and others identified that Gq/G11 and G12/G13 signaling to RhoA and Rho kinase in epithelial cells is central to the αvβ6 integrin–mediated activation of transforming growth factor–β (TGFβ) in vitro (3, 4). However, the importance of heterotrimeric G protein signaling pathways in the activation of TGFβ in the alveoli in vivo has not been described.

TGFβ plays a central role in diverse physiological processes, including homeostasis, repair, and immunity. The essential role of TGFβ in maintaining alveolar homeostasis was demonstrated in mice with defective TGFβ signaling pathways. Mice deficient in Smad3 (5), a major intracellular signal transducer and transcriptional modulator of TGFβ signaling, or the epithelial TGFβ receptor subunit TGFβRII (6) develop age-related emphysema because of increased production of matrix metalloprotease-12 (MMP12) by alveolar macrophages. Furthermore, over-expression of TGFβ in the lung leads to pulmonary fibrosis (7), and

increased TGFβ abundance is associated with the development of acute and ventilator-associated lung injury (8, 9). Disruption of alveolar TGFβ signaling also leads to human disease. Mutations in TGFβ1 and its receptors, as well as reduced serum concentrations of TGFβ1 are associated with the development of chronic obstructive pulmonary disease (COPD) (10-12). Furthermore, increased TGFβ signaling in the alveoli is associated with conditions such as idiopathic pulmonary fibrosis (IPF) (13). Therefore, precise control of alveolar TGFβ activity is central to the homeostatic function of pulmonary alveoli. Activation of the latent TGFβ complex is the rate-limiting step in TGFβ biosynthesis, and it is mediated in cells in vitro by a number of distinct mechanisms, including physical changes such as low pH or oxidation, proteases (14-16), or through the direct physical interaction of the extracellular domain of integrins with the RGD-binding site in the latent TGFβ binding protein (17-19). Studies in mice suggest that in vivo, in development at least, most pulmonary TGFβ1 activation is through both the $\alpha_v\beta_6$ and $\alpha_v\beta_8$ integrins (20, 21). Furthermore, mice with no functional $\alpha_v\beta_6$ integrins develop MMP12-dependent, age-related emphysema (22), consistent with observations from mice with defective TGFβ signaling.

To investigate the whether G protein signaling pathways were required to generate alveolar TGFβ and control alveolar homeostasis, mice were generated that were deficient in both $G\alpha_q$ and $G\alpha_{11}$ ($G\alpha_q/G\alpha_{11}$) or in both $G\alpha_{12}$ and $G\alpha_{13}$ ($G\alpha_{12}/G\alpha_{13}$) surfactant protein C (SftpC)-positive cells, restricting the defect in signaling predominantly to type II alveolar (ATII) epithelium. We showed that alveolar epithelial Gq/G11 signaling was required not only to promote stretch-mediated production of TGFβ by epithelial cells within the lungs, but also to suppress synthesis of the key epithelial alarmin interleukin-33 (IL-33) and inhibit the M2 polarization of alveolar macrophages. Loss of signaling through this pathway leads to emphysematous changes in the lungs because of the disruption of epithelial cell–mediated

suppression of macrophage activation and the resulting widespread alveolar destruction, but protected against stretch-mediated lung injury.

Results

Characterization of mice deficient in $G\alpha_q/G\alpha_{11}$ or $G\alpha_{12}/G\alpha_{13}$ in surfactant protein C–positive epithelial cells

To assess the role of the Gq/G11 and G12/G13 signaling pathways in alveolar epithelial cell function, two strains of mice were generated by Cre-loxP recombination. Mice heterozygous for the expression of Cre-recombinase under the control of the *surfactant protein C* promoter (*SftpC*$^{+/-}$) were crossed with mice either constitutively deficient in the gene encoding Gα11 (*Gna11*$^{-/-}$) and carrying floxed alleles of the gene encoding Gαq (*Gnaq*$^{fl/fl}$) (23) or constitutively deficient in the gene encoding Gα12 (*Gna12*$^{-/-}$) and carrying floxed alleles of the gene encoding Gα13 (*Gna13*$^{fl/fl}$) (24) to generate alveolar epithelial cell–specific, double knockout mice termed *SftpC*$^{+/-}$;*Gnaq*$^{fl/fl}$;*Gna11*$^{-/-}$ and *SftpC*$^{+/-}$;*Gna12*$^{-/-}$;*Gna13*$^{fl/fl}$, respectively. *SftpC*$^{+/-}$;*Gnaq*$^{fl/fl}$;*Gna11*$^{-/-}$ progeny were born at the expected Mendelian ratios from regular matings of founder animals. In contrast, the litter sizes of mice in the *SftpC*$^{+/-}$;*Gna12*$^{-/-}$;*Gna13*$^{fl/fl}$ colony were smaller and animals were not born at the expected Mendelian frequency (12.5% of each genotype), with only 6.8% of offspring being Cre-positive and carrying two null *Gna12* alleles and two floxed *Gna13* alleles.

Gαq/Gα11 colony mice were genotyped by PCR analysis (fig. S1A). Cre-mediated deletion of *Gnaq* in the alveolar cells of *SftpC*$^{+/-}$;*Gnaq*$^{fl/fl}$;*Gna11*$^{-/-}$ mice was confirmed by a reduction in the abundances of $G\alpha_q$ protein (fig. S1B) and mRNA (fig. S1C) compared with those of alveolar type II (ATII) cells isolated from Cre-negative *Gna11*$^{-/-}$ control mice. Immunohistochemical analysis of $G\alpha_q$ proteins demonstrated that the signaling molecule was

not detected in ATII cells from *SftpC*$^{+/-}$;*Gnaq*$^{fl/fl}$;*Gna11*$^{-/-}$ mice, but was detected in Cre-negative *Gna11*$^{-/-}$ mice (fig. S1D). Gα12/Gα13 colony mice were genotyped by PCR analysis (fig. S1E), and the Cre-mediated deletion of *Gna13* in the ATII cells of *SftpC*$^{+/-}$;*Gna12*$^{-/-}$;*Gna13*$^{fl/fl}$ mice was confirmed by immunohistochemical analysis of Gα13 protein (fig. S1F) and real time reverse-transcriptase PCR (RT-PCR) analysis of the abundance of *Gna13* mRNA in ATII cells (fig. S1G).

Gq/11-deficient mice have alveolar airspace enlargement and an obstructive lung defect

Analysis of the lungs from *SftpC*$^{+/-}$;*Gnaq*$^{fl/fl}$;*Gna11*$^{-/-}$ mice (Fig. 1A) revealed that they were morphologically normal at two weeks of age, although by four weeks there were widespread inflammatory infiltrates and architectural distortion within the lungs. There was enhanced inflammation and localized disruption of the alveolar architecture at six weeks, and this was maximal at eight weeks of age. Mean linear intercept analysis confirmed that substantial increases in alveolar size were not detected in the *SftpC*$^{+/-}$;*Gnaq*$^{fl/fl}$;*Gna11*$^{-/-}$ mice until they were four weeks of age (Fig. 1B), and that these animals subsequently showed a progressive and age-related increase in the size of the alveoli up to eight weeks of age compared with age-matched *Gna11*$^{-/-}$ control mice. Although there was no further increase in mean linear intercept beyond eight weeks, alveolar size remained substantially greater in *SftpC*$^{+/-}$;*Gnaq*$^{fl/fl}$;*Gna11*$^{-/-}$ mice than in *Gna11*$^{-/-}$ mice up to six months of age (Fig.1B). In contrast with that of *SftpC*$^{+/-}$;*Gnaq*$^{fl/fl}$;*Gna11*$^{-/-}$ mice, mean linear intercept analysis of lung sections from Cre-positive heterozygous Gαq/Gα11 colony mice and from *SftpC*$^{+/-}$;*Gna12*$^{-/-}$;*Gna13*$^{fl/fl}$ mice showed no evidence of increased alveolar airspace size (fig S2A) or inflammatory infiltrates (fig. S2, B to D). Even at the later time points of 12 and 24 weeks of age (fig. S2E), there was no evidence of inflammation or architectural distortion in the lungs of *SftpC*$^{+/-}$

;*Gna12*$^{-/-}$;*Gna13*$^{fl/fl}$ mice, suggesting that G12/G13 signaling does not play a role in the postnatal development of alveoli or in alveolar homeostasis.

To confirm that the morphological changes had functional consequences, lung function was measured by invasive plethysmography at eight weeks of age. *SftpC*$^{+/-}$;*Gnaq*$^{fl/fl}$;*Gna11*$^{-/-}$ mice showed an obstructive defect as evidenced by a statistically significant reduction in the ratio of forced expiratory volume in the first 100 ms (FEV100) to forced vital capacity (FVC), that is, the FEV100/FVC (Fig. 1C). A reduction in the FEV100/FVC ratio is characteristic of the development of emphysema together with increased static lung volumes as reflected by statistically significantly increased total lung capacity (TLC) (fig. S3A) and functional residual capacity (FRC) (fig. S3B) when compared with *Gna11*$^{-/-}$ mice. There was no significant increase in residual volume (RV) detected in the *SftpC*$^{+/-}$;*Gnaq*$^{fl/fl}$;*Gna11*$^{-/-}$ mice (fig. S3C). Leukocytes isolated from the bronchoalveolar lavage fluid (BALF) of *SftpC*$^{+/-}$;*Gnaq*$^{fl/fl}$;*Gna11*$^{-/-}$ mice had substantially increased amounts of *Mmp2* (Fig. 1D), *Mmp9* (Fig. 1E), and *Mmp12* (Fig. 1F) mRNAs compared with those of *Gna11*$^{-/-}$ mice, as determined by real time RT-PCR analysis, which suggests a contributory role for these enzymes in the alveolar destruction observed in the *SftpC*$^{+/-}$;*Gnaq*$^{fl/fl}$;*Gna11*$^{-/-}$ mice.

Loss of alveolar epithelial Gq/11 signaling leads to decreased activation of TGFβ in the lung

To determine whether TGFβ signaling pathways were disrupted by the loss of $G\alpha_q$ and $G\alpha_{11}$ from epithelial cells, we measured the total TGFβ1 concentrations in whole-lung homogenates and found them to be substantially decreased in *SftpC*$^{+/-}$;*Gnaq*$^{fl/fl}$;*Gna11*$^{-/-}$ mice compared to those in *Gna11*$^{-/-}$ control mice (Fig. 2A). Analysis of supernatants collected from cultured lung slices detected the release of active TGFβ from the *Gna11*$^{-/-}$ lung slices, but no

active TGFβ1 was measured in the supernatants of *SftpC*$^{+/-}$;*Gnaq*$^{fl/fl}$;*Gna11*$^{-/-}$ lung slices (Fig. 2B). To examine the role of Gαq and Gα11 in TGFβ activation in response to a contraction stimulus, lung slices were incubated with methacholine, which activates Gq/G11 signaling through muscarinic receptors. There was no substantial increase in the amount of active TGFβ detected in the lung slice supernatants of either genotype (Fig. 2B); however, treatment of slices from *Gna11*$^{-/-}$ mice with methacholine led to increased amounts of phosphorylated Smad2 (pSmad2) protein in lung slice lysates, which was not observed in the treated slices from *SftpC*$^{+/-}$;*Gnaq*$^{fl/fl}$;*Gna11*$^{-/-}$ animals (Fig. 2C).

To confirm that the reduction in total TGFβ generation observed was to the result of reduced alveolar TGFβ activation in vivo, BAL leukocytes were used as reporter cells for the activation of TGFβ in epithelial cells (Fig. 2D). Nuclear extracts of BAL leukocytes collected from *SftpC*$^{+/-}$;*Gnaq*$^{fl/fl}$;*Gna11*$^{-/-}$ mice had substantially less pSmad2 abundance than did the nuclear extracts of BAL leukocytes from *Gna11*$^{-/-}$ mice, thus confirming that the amount of active TGFβ produced by the lung epithelium was reduced in the *SftpC*$^{+/-}$;*Gnaq*$^{fl/fl}$;*Gna11*$^{-/-}$ mice (Fig. 2D). Furthermore, exogenous stimulation of BAL leukocytes from *SftpC*$^{+/-}$;*Gnaq*$^{fl/fl}$;*Gna11*$^{-/-}$ mice with TGFβ for 1 hour stimulated a small, although statistically significant, increase in pSmad2 abundance, which was considerably blunted compared with that observed in cells from *Gna11*$^{-/-}$ mice (Fig. 2D). RT-PCR analysis of the expression of two TGFβ-responsive genes, *Itgb6* (Fig. 2E) and *Tsp1* (Fig. 2F) demonstrated that ATII cells from *SftpC*$^{+/-}$;*Gnaq*$^{fl/fl}$;*Gna11*$^{-/-}$ mice had statistically significantly lower amounts of both mRNAs than did cells from *Gna11*$^{-/-}$ littermate controls.

Disruption of alveolar Gq/G11 signaling leads to aberrant alveolar macrophage responses

To investigate the mechanism behind the reduced responsiveness of BAL leukocytes from *SftpC*$^{+/-}$;*Gnaq*$^{fl/fl}$;*Gna11*$^{-/-}$ mice to TGFβ (Fig 2D), we measured the abundances of the mRNAs encoding TGFβ receptor I (*Tgfbr1*) and II (*Tgfbr2)*. *Tgfbr1* mRNA abundance was substantially reduced in BAL macrophages from *SftpC*$^{+/-}$;*Gnaq*$^{fl/fl}$;*Gna11*$^{-/-}$ mice compared to that in cells from *Gna11*$^{-/-}$ littermate control mice (Fig. 3A). In contrast, the abundance of *Tgfbr2* mRNA was increased in the cells isolated from *SftpC*$^{+/-}$;*Gnaq*$^{fl/fl}$;*Gna11*$^{-/-}$ mice, although this difference did not reach statistical significance (Fig. 3A). To determine whether TGFβR abundance in BAL macrophages was regulated by factors secreted into the alveolar compartment, crossover experiments were performed in which BAL macrophages from *Gna11*$^{-/-}$ mice or *SftpC*$^{+/-}$;*Gnaq*$^{fl/fl}$;*Gna11*$^{-/-}$ mice were cultured with BALF from either *Gna11*$^{-/-}$ mice or *SftpC*$^{+/-}$;*Gnaq*$^{fl/fl}$;*Gna11*$^{-/-}$mice and then *Tgfbr* mRNA abundances were assessed. *Tgfbr* mRNA abundance was measured in BAL macrophages from *SftpC*$^{+/-}$;*Gnaq*$^{fl/fl}$;*Gna11*$^{-/-}$ animals cultured in BALF from *SftpC*$^{+/-}$;*Gnaq*$^{fl/fl}$;*Gna11*$^{-/-}$ mice or *Gna11*$^{-/-}$ mice, and exposure of *SftpC*$^{+/-}$;*Gnaq*$^{fl/fl}$;*Gna11*$^{-/-}$ macrophages to BALF from *Gna11*$^{-/-}$ mice for 24 hours induced a statistically significant increase in macrophage *Tgfbr1* expression, which was blocked by concomitant administration of an anti-TGFβ blocking antibody (Fig. 3B). Stimulation of BAL macrophages from *SftpC*$^{+/-}$;*Gnaq*$^{fl/fl}$;*Gna11*$^{-/-}$ mice with TGFβ induced a substantial increase in *Tgfbr1* mRNA abundance, which confirms a role for TGFβ in regulating the expression of its own receptor (Fig. 3C). To assess the consequences of reduced alveolar TGFβ activation on BAL macrophages from *SftpC*$^{+/-}$;*Gnaq*$^{fl/fl}$;*Gna11*$^{-/-}$mice, we measured *Mmp12* mRNA abundance. Culturing alveolar macrophages, obtained from the BAL from *Gna11*$^{-/-}$ mice in BALF from the *SftpC*$^{+/-}$;*Gnaq*$^{fl/fl}$;*Gna11*$^{-/-}$mice induced the expression of *Mmp12* in these cells. This increase was markedly inhibited by co-stimulation with exogenous TGFβ (Fig. 3D) suggesting that the Gq/11-dependent generation of TGFβ from epithelial cells is required to suppress macrophage MMP12 production and prevent the

development of emphysema. In contrast, co-administration of an anti-TGFβ blocking antibody led to a trend towards increased *Mmp12* mRNA abundance (Fig 3E), but this was not statistically significant.

Loss of Gq/G11 signaling leads to inflammatory cell recruitment and the M2 polarization of alveolar macrophages

A characteristic feature of *SftpC*$^{+/-}$;*Gnaq*$^{fl/fl}$;*Gna11*$^{-/-}$ mice was the appearance of enlarged and vacuolated cells within the alveolar airspaces (Fig. 4A), which stained positive for the macrophage marker F4/80 (Fig. 4B). *SftpC*$^{+/-}$;*Gnaq*$^{fl/fl}$;*Gna11*$^{-/-}$ mice had a 10-fold increase in the total numbers of leukocytes within the alveolar airspaces compared with *Gna11*$^{-/-}$, Cre-positive heterozygous littermate controls or *SftpC*$^{+/-}$;*Gna12*$^{-/-}$;*Gna13*$^{fl/fl}$ mice (Fig. 4C). Cytospin analysis of BALF from the *SftpC*$^{+/-}$;*Gnaq*$^{fl/fl}$;*Gna11*$^{-/-}$ animals confirmed the increased numbers of enlarged, vacuolated cells (Fig. 4D), which were not observed in the cytospins from any other genotype and were made up of approximately 50% of the cells within the BALF (Fig. 4E). Phenotypic analysis revealed a heterogeneous population of macrophages with widespread distribution of M2-like markers, including resistin-like molecule α (RELMα; M2a) and mannose receptor (M2a/c) together with a more restricted pattern of sphingosine kinase (Sphk1; M2b) positivity in the BAL cells isolated from *SftpC*$^{+/-}$;*Gnaq*$^{fl/fl}$;*Gna11*$^{-/-}$ mice (Fig 4F). Quantification of the immunofluorescence staining confirmed the increased amounts of all three M2 macrophage markers. Although there was a statistically significant increase in the abundance of inducible nitric oxide synthase (iNOS) in the *SftpC*$^{+/-}$;*Gnaq*$^{fl/fl}$;*Gna11*$^{-/-}$ BAL cells, most of the enlarged macrophages did not contain iNOS, suggesting that they had an M2 phenotype (Fig. 4F). Further analysis also demonstrated that macrophages from *SftpC*$^{+/-}$;*Gnaq*$^{fl/fl}$;*Gna11*$^{-/-}$ animals contained

significantly more IL-10 than did macrophages from *Gna11*$^{-/-}$ mice (Fig. 4G), which is consistent with their polarization to an M2 phenotype.

Disruption of alveolar epithelial Gq/G11 signaling leads to increased IL-33 production

To determine the effect of disrupting alveolar epithelial Gq/G11 and G12/G13 signaling on global gene networks, Affymetrix gene chip analysis was performed on mRNA isolated from alveolar epithelial cells from *Gna11*$^{-/-}$, *SftpC*$^{+/-}$;*Gnaq*$^{fl/fl}$;*Gna11*$^{-/-}$, *Gna12*$^{-/-}$, and *SftpC*$^{+/-}$;*Gna13*$^{fl/fl}$;*Gna12*$^{-/-}$ mice. Affymetrix analysis compared gene expression in *SftpC*$^{+/-}$;*Gnaq*$^{fl/fl}$;*Gna11*$^{-/-}$ cells with that in four different comparator groups, namely: (i) *Gna11*$^{-/-}$ mice alone; (ii) *SftpC*$^{+/-}$;*Gna13*$^{fl/fl}$;*Gna12*$^{-/-}$ mice alone; (iii) *Gna11*$^{-/-}$ mice and *Gna12*$^{-/-}$ mice combined; and (iv) *Gna11*$^{-/-}$ mice, *Gna12*$^{-/-}$ mice, and *SftpC*$^{+/-}$;*Gna13*$^{fl/fl}$;*Gna12*$^{-/-}$ mice combined. Using the data obtained from all four contrasting genotypes we identified 304 probes that mapped to 256 genes (see supplementary data file S1) that were differentially expressed in the *SftpC*$^{+/-}$;*Gnaq*$^{fl/fl}$;*Gna11*$^{-/-}$ epithelial cells regardless of the comparator group used. Hierarchical cluster analysis of the differentially expressed genes showed separation between epithelial cells from the *SftpC*$^{+/-}$;*Gnaq*$^{fl/fl}$;*Gna11*$^{-/-}$mice and epithelial cells from mice of all other genotypes (Fig. 5A), reflecting the differences observed in the pulmonary phenotype. Ingenuity Pathway Analysis suggested increased activation of signal transducer and activator of transcription 6 (STAT6) pathways terminating in enhanced IL-33 production in the *SftpC*$^{+/-}$;*Gnaq*$^{fl/fl}$;*Gna11*$^{-/-}$ alveolar epithelial cells compared with that in alveolar epithelial cells from *Gna11*$^{-/-}$ control mice, which was confirmed by Western blotting analysis (Fig. 5B).

Immunohistochemical analysis of lung tissue detected increased IL-33 abundance in the nuclei of ATII cells from *SftpC*$^{+/-}$;*Gnaq*$^{fl/fl}$;*Gna11*$^{-/-}$ mice compared with that in the nuclei of

ATII cells from *Gna11*$^{-/-}$ mice (Fig. 5, C and D). Cytoplasmic IL-33 was present only in alveolar epithelial cells from *SftpC*$^{+/-}$;*Gnaq*$^{fl/fl}$;*Gna11*$^{-/-}$ mice (Fig. 5, C and D). Concentrations of IL-33 in lung homogenates from *SftpC*$^{+/-}$;*Gnaq*$^{fl/fl}$;*Gna11*$^{-/-}$ mice were statistically significantly greater than those in lung homogenates from *Gna11*$^{-/-}$ mice (Fig. 5E). In contrast, concentrations of the T helper 2 (T_H2)-type cytokines IL-4, IL-10, and IL-13 were similar between *SftpC*$^{+/-}$;*Gnaq*$^{fl/fl}$;*Gna11*$^{-/-}$ mice and *Gna11*$^{-/-}$ mice (fig. S4, A to C). Although the amount of the soluble IL-33 receptor ST2 was not substantially increased in lung tissue homogenates (fig. S4D), it was markedly increased in the BALF from *SftpC*$^{+/-}$;*Gnaq*$^{fl/fl}$;*Gna11*$^{-/-}$ mice compared with that in the BALF from *Gna11*$^{-/-}$ mice, suggesting that IL-33 was secreted into the extracellular compartment (Fig. 5F). The concentrations of IL-33 in the lungs of mice deficient in *Itgb6* (which encodes the β_6 integrin subunit) were not substantially different from those in the lungs of wild-type mice (Fig. 5G), suggesting that $\alpha_v\beta_6$ integrin–mediated activation of TGFβ was not required to suppress IL-33 production.

The increased IL-33 production from Gq/11-deficient epithelial cells promotes the polarization of alveolar macrophages to an M2 phenotype

To assess the role of IL-33 in M2 macrophage polarization, alveolar macrophages from *Gna11*$^{-/-}$ mice were cultured in BALF from *SftpC*$^{+/-}$;*Gnaq*$^{fl/fl}$;*Gna11*$^{-/-}$ mice, which resulted in a substantial increase in *Il10* mRNA abundance (Fig. 6A). Concomitant treatment with exogenous TGFβ had no effect on *Il10* mRNA abundance; however, the induction of *Il10* mRNA expression was completely inhibited by an anti-IL-33 blocking antibody (Fig. 6A). Similarly, exposure of *Gna11*$^{-/-}$ macrophages to BALF from *SftpC*$^{+/-}$;*Gnaq*$^{fl/fl}$;*Gna11*$^{-/-}$ mice resulted in a trend towards increased *Arginase 1* (*Arg1;* M2a/c*)* and *Sphk1* mRNA abundances (characteristic of M2 macrophages), although these differences were not statistically significant (Fig. 6B). Neutralization of IL-33 in the BALF from *SftpC*$^{+/-}$

;*Gnaq*$^{fl/fl}$;*Gna11*$^{-/-}$ mice blocked the increase in *Arg1* and *Sphk1* mRNA abundances in the alveolar macrophages (Fig. 6B). Furthermore, culturing alveolar macrophages from *Gna11*$^{-/-}$ mice in the BALF from *SftpC*$^{+/-}$;*Gnaq*$^{fl/fl}$;*Gna11*$^{-/-}$ mice for 24 hours lead to the increased abundance of the M2a macrophage marker RELMα, as measured by immunofluorescence, which was substantially inhibited in the presence of an anti-IL-33 blocking antibody (Fig. 6, C and D). Together, these date suggest that the M2 macrophage polarization in the *SftpC*$^{+/-}$;*Gnaq*$^{fl/fl}$;*Gna11*$^{-/-}$ mice is driven by the increased production of IL-33 by alveolar epithelial cells.

Gq/11 signaling in alveolar epithelial cells transduces stretch-mediated generation of TGFβ in the lungs

To assess the role of alveolar epithelial Gq/G11 signaling in stretch-mediated TGFβ generation, *Gna11*$^{-/-}$ mice and *SftpC*$^{+/-}$;*Gnaq*$^{fl/fl}$;*Gna11*$^{-/-}$ mice were exposed to high pressure ventilation to induce ventilator-induced lung injury (VILI). Mice of each genotype were ventilated for 60 min to a standardized plateau pressure (*Gna11*$^{-/-}$ mice: 37.93 ± 037 cm H_2O; *SftpC*$^{+/-}$;*Gnaq*$^{fl/fl}$;*Gna11*$^{-/-}$ mice: 37.83 ± 038 cm H_2O) that was designed to impart an equivalent degree of mechanical stress and stretch to each set of lungs. This period of high-pressure ventilation (V_T) was followed by 3 hours of non-injurious ventilation. *Gna11*$^{-/-}$ mice showed statistically significant increases in peak inspiratory pressure (Fig. 7A), plateau pressure (Fig. 7B), and lung elastance (Fig. 7C) after exposure to high V_T, which is indicative of the development of lung injury. In contrast, *SftpC*$^{+/-}$;*Gnaq*$^{fl/fl}$;*Gna11*$^{-/-}$ mice were protected from the development of physiological responses associated with ventilator-induced lung injury (Fig. 7, A to C). There was no statistically significant difference in lung resistance between the two genotypes of mice (Fig. 7D).

Protection from the development of ventilator-induced lung injury in *SftpC*$^{+/-}$;*Gnaq*$^{fl/fl}$;*Gna11*$^{-/-}$ mice was linked to the inability of these animals to generate TGFβ1 in response to mechanical stretch (Fig. 7E). Lung TGFβ1 concentrations were substantially increased in *Gna11*$^{-/-}$ animals exposed to short-term, high-stretch ventilation compared with those in animals exposed to only non-injurious low ventilation pressures for 4 hours. These stretch-induced increases in TGFβ1 were completely abrogated in *SftpC*$^{+/-}$;*Gnaq*$^{fl/fl}$;*Gna11*$^{-/-}$ mice. Although IL-33 concentrations were statistically significantly greater in the lungs of *SftpC*$^{+/-}$;*Gnaq*$^{fl/fl}$;*Gna11*$^{-/-}$ mice than in the lungs of their *Gna11*$^{-/-}$ littermate controls, IL-33 production in the lungs was not dependent on alveolar epithelial stretch (Fig. 7F), suggesting that Gq/G11 signaling has non-overlapping effects on the TGFβ and IL-33 signaling pathways.

Discussion

The aim of this study was to investigate the role of two key G protein signaling pathways, those mediated by Gq/G11 and G12/G13, in the regulation of alveolar epithelial homeostasis, and to understand the pathological consequences of disrupting these pathways within the alveoli. Because of the functional redundancy of closely related G proteins and the induction of compensatory processes, it was necessary to perform studies in animals in which pairs of G proteins were deleted. Embryonic lethality has been reported in both Gq/G11 (23) and G12/G13 (25) knockout animals; therefore, a cell-targeted approach was required in which pairs of G proteins were deleted only in SftpC-positive epithelial cells within the lung. Comparisons were made with *Gna11*$^{-/-}$ or *Gna12*$^{-/-}$ Cre-negative littermate control mice, which previously had no reported lung abnormalities.

We did not find any phenotype associated with the alveolar deletion of both *Gna12* and

Gna13 with respect to lung development. Similarly, we did not find any phenotype associated with *Gna11*$^{-/-}$ animals, although we cannot exclude a role for these G proteins in response to lung injury. We did, however, show that deletion of both $G\alpha_q$ and $G\alpha_{11}$ in SftpC-positive ATII cells led to a phenotype of impaired TGFβ signaling and enhanced IL-33 production. This resulted in M2 macrophage polarization and the increased expression of *Mmp12* by macrophages, which resulted in changes within the lungs, including inflammation and alveolar airspace enlargement consistent with emphysema. Although we cannot completely exclude the possibility that the observed phenotype was primarily because of the alveolar deletion of *Gnaq*, we believe that this is unlikely for a number of reasons. First, most genetic models have not demonstrated any evidence of defects in the absence of $G\alpha_q$ alone. In the few cases in which $G\alpha_q$ deficiency promotes abnormalities, such as defective platelet activation (26) and the development of cerebellar ataxia (27), this is because $G\alpha_{11}$ is not found in platelets (26) or is present at relatively low abundance in Purkinje cells (28). Second, these observations are consistent with biochemical data showing that GPCRs do not distinguish between $G\alpha_q$ and $G\alpha_{11}$ (29-32) and that both G proteins regulate the same effectors (33, 34). Therefore, it is likely that the observed phenotype is the result of deletion of both the $G\alpha_q$ and $G\alpha_{11}$ signaling molecules.

We determined that impaired Gq/G11 signaling in alveolar epithelial cells led to two nonredundant, non-overlapping consequences in the alveoli. First, we observed reduced stretch-mediated TGFβ1 generation in the alveoli as measured by reduced TGFβ1 release in vivo, in addition to decreased amounts of active TGFβ and pSmad2, which were measured ex vivo in methacholine-treated lung slices from *SftpC*$^{+/-}$;*Gnaq*$^{fl/fl}$;*Gna11*$^{-/-}$ mice. This deficiency in TGFβ production in the alveoli ultimately resulted in altered macrophage functioning because of a reduction in *Tgfbr1* expression and an increase in *Mmp12* expression in alveolar

macrophages. Second, we identified increased synthesis of IL-33 by alveolar epithelial cells, which promoted the polarization of alveolar macrophages towards an M2 phenotype in ex vivo experiments. These data confirm our previous in vitro findings that suggest that Gq/G11 signaling is crucial for mediating the activation of TGFβ in alveolar epithelial cells (4), and highlight a hitherto unknown role for alveolar Gq/G11 signaling in suppressing IL-33 production and maintaining alveolar macrophage homeostasis. It is likely that the Gq/G11-dependent generation of TGFβ and suppression of IL-33 production is a fundamental pathway in the epithelium. Previous studies of mice deficient in Rac1 (a downstream effector of Gq/G11 signaling) specifically in airway epithelial cells demonstrated enhanced inflammatory responses, impaired TGFβ production, and exaggerated IL-33–dependent responses (35), with which our data are consistent. Moreover, the intestinal helminth *Heligmosomoides polygyrus* secretes proteins that induce TGFβ signaling (36) and inhibit IL-33 (37), thus mimicking the effect of epithelial Gq/G11 signaling.

Previous in vivo studies that have attenuated TGFβ signaling in the lung, either through whole-body deletion of Smad3 (5) or $\alpha_v\beta_6$ integrins (22, 38) or through epithelial cell–specific deletion of TGFβRII (6), have shown mild pulmonary inflammation, epithelial airspace enlargement, and enhanced *Mmp12* expression, consistent with our findings with the *SftpC*$^{+/-}$;*Gnaq*$^{fl/fl}$;*Gna11*$^{-/-}$ mice. However, the degree of inflammation and airspace destruction observed in the lungs of *SftpC*$^{+/-}$;*Gnaq*$^{fl/fl}$;*Gna11*$^{-/-}$ mice was considerably worse at an earlier stage of development than that reported in the previous studies. It is possible that the combination of increased expression of *Mmp9* and *Mmp12* within the BAL leukocytes of the *SftpC*$^{+/-}$;*Gnaq*$^{fl/fl}$;*Gna11*$^{-/-}$ mice may contribute to the exaggerated response seen in these animals, because both effects may play a role in the development of emphysema (22, 39). However, we believe that the severe phenotype most likely results from the combined effects

of a failure of TGFβ activation on alveolar epithelial cells and an increase in their production of IL-33. IL-33 is associated with enhanced pulmonary inflammation and increased generation of ST2 and IL-10 (40) in addition to promoting the polarization of macrophages toward an alternatively activated (M2) state (41, 42). Increased epithelial IL-33 has also previously been linked to the development of COPD (43).

These data demonstrate that *SftpC*$^{+/-}$;*Gnaq*$^{fl/fl}$;*Gna11*$^{-/-}$ mice have reduced amounts of TGFβ in their lungs which, in contrast with *Gna11*$^{-/-}$ mice, could not be increased in response to epithelial cell stretch after high-pressure ventilation in vivo or methacholine-induced contraction ex vivo. This is consistent with a failure of $\alpha_v\beta_6$ integrin–mediated activation of TGFβ, which requires force generation through RhoA-induced intracellular cytoskeletal reorganization (4, 44, 45). The phenotype of impaired $\alpha_v\beta_6$ integrin–mediated TGFβ activation is further supported by the reduced abundance of pSmad2 in alveolar macrophages and the reduced abundance of *itgb6* mRNA in alveolar epithelial cells from *SftpC*$^{+/-}$;*Gnaq*$^{fl/fl}$;*Gna11*$^{-/-}$ mice. Our previous findings suggested a critical role for $G\alpha_q$ in the regulation of $\alpha_v\beta_6$ integrin–mediated TGFβ activation independently of the abundance of $\alpha_v\beta_6$ (4). However, TGFβ signaling increases the epithelial cell abundance of $\alpha_v\beta_6$ integrin by inducing *itgb6* expression (46), which has led to the proposal of a TGFβ–$\alpha_v\beta_6$ integrin positive feed-forward loop (47). These data support this hypothesis, because sustained reduction of alveolar TGFβ activation in the *SftpC*$^{+/-}$;*Gnaq*$^{fl/fl}$;*Gna11*$^{-/-}$ mice led to reduced *itgb6* expression in alveolar epithelial cells.

Itgb6$^{-/-}$ mice are protected from the development of ventilator-induced lung injury (9), and our data demonstrate that *SftpC*$^{+/-}$;*Gnaq*$^{fl/fl}$;*Gna11*$^{-/-}$ mice are also protected from the deleterious effects of high-pressure ventilation, suggesting that Gq/11 signaling pathways are

crucial for epithelial mechanotransduced signals that promote TGFβ activation. Furthermore, we observed that airspace enlargement in the *SftpC*$^{+/-}$;*Gnaq*$^{fl/fl}$;*Gna11*$^{-/-}$ mice developed postnatally, when spontaneous ventilation began, and was not apparent until the mice were four weeks of age. Therefore, we propose the hypothesis that spontaneous ventilation leads to cyclical alveolar stretch and the release of GPCR ligands that act through the Gq/G11 pathway to promote alveolar TGFβ activation, suppress macrophage *Mmp12* expression, and prevent the subsequent development of emphysema. However, further evidence is required to determine whether the stretch-induced production of TGFβ is directly linked to TGFβ activation by the $\alpha_v\beta_6$ integrin.

We suggest that Gq/G11 signaling has non-overlapping effects on TGFβ activation and IL-33 production. Although previous studies have suggested that IL-33 is a mechanically stimulated cytokine (48), we found no evidence that IL-33 production in the lungs was regulated by exposure to epithelial cell stretch. Therefore, it is likely that the enhanced IL-33 generation observed in the *SftpC*$^{+/-}$;*Gnaq*$^{fl/fl}$;*Gna11*$^{-/-}$ mice was driven by transcriptional signals rather than by mechanotransduction. TGFβ limits the production of IL-33 by macrophages (49); therefore, it is possible that the observed increase in IL-33 abundance in the *SftpC*$^{+/-}$;*Gnaq*$^{fl/fl}$;*Gna11*$^{-/-}$ mice was a result of reduced TGFβ activity in the alveoli. However, we do not favor this hypothesis because, in contrast to the findings in the *SftpC*$^{+/-}$;*Gnaq*$^{fl/fl}$;*Gna11*$^{-/-}$ mice, we did not observe any change in IL-33 concentrations in the lungs of *Itgb6*$^{-/-}$ mice.

In summary, our findings suggest that Gq/G11 signaling is required for two non-overlapping signaling pathways: the mechanotransduced generation of TGFβ and the transcriptional suppression of IL-33, both of which appear to be essential for the maintenance of alveolar macrophage homeostasis. Enhanced IL-33 production promotes the polarization of the

alveolar macrophages to an M2 phenotype, whereas the failure of epithelial cells to generate TGFβ led to impaired *Tgfbr1* expression in alveolar macrophages and the loss of TGFβ–mediated suppression of MMP12 production by macrophages. Loss of the homeostatic control of alveolar macrophages results in widespread alveolar destruction and airspace enlargement associated with the development of emphysema. These data confirm the central role of Gq/G11 signaling in stretch-mediated alveolar TGFβ generation in vivo, reveal a hitherto unknown role for Gq/G11 signaling in the regulation of IL-33 by epithelial cells, and highlight a molecular pathway that is required to prevent ventilation-associated alveolar disease.

Material and Methods

Study design

All animal experiments were designed to test a specific hypothesis or objective, with data being recorded and reported in accordance with the guidelines from the Fund for The Replacement of Animals in Medical Experiments (FRAME) and Animal Research: Reporting of In Vivo Experiments (ARRIVE). Phenotyping experiments were performed blind to genotype to minimize bias and with a factorial design to minimize confounding variables. Animals were assigned a six-digit identity code at weaning and were genotyped before analysis, but data collection was performed by researchers blinded to genotype. Initial studies were performed to establish the baseline phenotype of the mice and the variability of observed biochemical, morphological, and physiological parameters. For ventilator-induced lung injury and lung function experiments, mice were assigned to experimental groups based on genotype; however, experimental procedures, data collection, and analysis were performed by an investigator blinded to the allocation sequence and genotype. Studies were powered to detect a 1 standard deviation difference in endpoints using a power calculation

assuming an 80% power at the 5% significance level, resulting in group sizes of 5 to 8 mice per group based on initial phenotyping data. Sample sizes were pre-determined for in vitro studies with isolated primary cells, including RNA analysis and gene array studies and based on large expected effect sizes required three to six mice of each genotype.

Experimental animals

Mice were housed under specific pathogen–free conditions, and all animal experiments were performed in accordance with the U.K. Animals (Scientific Procedures) Act 1986 and approved by the Animal Welfare and Ethical Review Committee at the University of Nottingham. The generation of floxed alleles of the genes encoding Gαq (*Gnaq*) and Gα13 (*Gna13*) and of the null alleles for the genes encoding Gα11 (*Gna11*) and Gα12 (*Gna12*) has been described previously (23, 24). Mice constitutively deficient in *Gna11* and containing floxed alleles of *Gnaq* or mice constitutively deficient in *Gna12* and containing floxed alleles of *Gna13* were crossed with mice expressing Cre recombinase under the control of the Surfactant Protein C promoter (*SftpC*-Cre) obtained from Brigid Hogan, Duke University (50). Mice were genotyped from DNA isolated from ear notch biopsies by polymerase chain reaction (PCR) analysis with allele-specific primers (table S1) and analyzed by electrophoresis on ethidium bromide–stained agarose gels as previously described (23, 24). The genetic background of the mice was predominantly C57BL6 (at least a sixth-generation backcross for Gαq/Gα11 and Gα12/Gα13 mice and at least fourth-generation backcross for *SftpC*-Cre mice).

Antibodies

Anti-mouse Gαq (Clone E17, sc-393, Santa Cruz Biotechnology, UK) and anti-IL-33 (Clone Nessy-1, ab54385, Abcam, UK) antibodies were used for Western blotting analysis. The

following antibodies for immunohistochemistry or immunofluorescence staining were purchased from Abcam: anti-Sphk1 (ab71700), anti-mouse iNos (ab15323), anti-mouse RELMα (ab39626), anti-mouse IL-10 (ab9969), anti-mouse Gnaq (ab128060), and anti-Gα13 (Clone EPR5436). Anti-mouse CD206 (Mannose Receptor) was obtained from Serotec, UK (MCA225). Anti-mouse IL-33 (AF3626) and anti-TGFβ-1,2,3 blocking antibody (clone 1D11) were purchased from R&D systems, UK. Anti-IL-33 (Bondy-1-1) blocking antibody was from Caltag Medsystems Ltd, UK. Biotinylated or Dylight488- and Dylight649-labelled secondary antibodies were purchased from VectorLabs and Jackson ImmunoResearch, respectively. Horseradish peroxidase (HRP)-conjugated secondary antibodies for Western blotting analysis were obtained from Dako, UK.

Quantitative morphometry and mean linear intercept

Mice were terminally anaesthetized with Euthatal (Merial Animal Health, UK) and the lungs and trachea were exposed. The lungs were perfused with phosphate-buffered saline (PBS) containing heparin (40 U/ml) through the left ventricle to remove all of the blood before the trachea was cannulated. Lungs were insufflated in situ with 10% neutral-buffered formalin at a constant pressure of 20 cm H_2O, removed, and paraffin-embedded for the preparation of histological sections. Lung morphology was assessed in hematoxylin and eosin–stained 5-μm tissue sections. For each set of lungs, eight random fields were photographed across all lobes with a Nikon Eclipse 90i microscope at 10x magnification and NIS Elements Software v3.2. Images were overlaid with a 100-μm grid, and the mean linear intercept [defined as the linear sum of the lengths, in μm, of all lines in all frames counted divided by the number of intercepts (defined as an alveolar septa intersecting with a counting line)] was calculated with a method adapted from Dunnill (51).

Lung function measurements by forced pulmonary maneuvers

Eight-week-old mice were anesthetized with an intraperitoneal injection of ketamine (75 mg/kg) and medetomidine hydrochloride (1 mg/kg) to maintain spontaneous breathing under anesthesia. Mice were tracheostomized, placed in a body plethysmograph, and connected to a computer-controlled ventilator (Forced pulmonary maneuver system; Buxco Research Systems, USA). An average breathing frequency of 120 breaths/min was imposed on the anesthetized animal by pressure-controlled ventilation until a regular breathing pattern and complete expiration at each breathing cycle were obtained. To measure functional residual capacity (FRC), ventilation was stopped at the end of expiration through the immediate closure of a valve located proximally to the endotracheal tube. Pressure changes at the mouth and in the bodybox after spontaneous breathing maneuvers against a closed valve were recorded to calculate the FRC (Boyle's law). To measure the total lung capacity (TLC), residual volume (RV), inspiratory capacity (IC), and vital capacity (VC), the quasistatic pressure volume maneuver was performed. In this maneuver, the lungs are inflated to a standard pressure of +30 cm H_2O, which was followed by a slow exhalation until a negative pressure of -30 cmH_2O was reached. The quasi-static compliance was defined as the volume:pressure ratio at 50% of the expiration (Cchord50). For the fast flow volume maneuver, lungs were first inflated to +30 cm H_2O (TLC) and immediately afterwards connected to a highly negative pressure to enforce expiration until the RV reached –30 cm H_2O. Forced expiratory flows (PEF and FEF), times of expiration and inspiration (Te, Ti), and forced expiratory volumes (forced expiratory volume at 100 and 200 ms, FEV100 and FEV200, respectively) were recorded during this maneuver. Suboptimal maneuvers were rejected, and for each test in every single mouse at least three acceptable maneuvers were conducted to obtain a reliable mean for all numeric parameters.

Ventilator-induced lung injury

Mice were anesthetized (80 mg/kg ketamine:8 mg/kg xylazine) and surgically instrumented for ventilation as described in detail previously (52) by an experimenter blinded to genotype. In brief, animals were tracheostomized and connected to a custom-made ventilator/pulmonary function testing system. The left carotid artery was cannulated to enable continual monitoring of arterial blood pressure, removal of samples for blood gas analysis at predetermined intervals, and infusion of fluids [heparin (10 U/ml) in 0.9% NaCl, 0.3 ml/hour]. During surgery and the subsequent stabilization period, mice were ventilated with a noninjurious strategy [8 to 9 ml/kg tidal volume (V_T), 3 cm H_2O positive end expiratory pressure (PEEP), 120 breaths per minute] using 100% O_2. Lung volume history was standardized by sustained inflation, and baseline respiratory mechanics were evaluated by the end-inflation occlusion technique. After baseline measurements were made, V_T was increased to produce stretch-induced lung injury. Specifically, ventilation was standardized with a plateau pressure of 37.5 to 38.5 cm H_2O, which was designed to ensure that mice of different genotypes were exposed to an equivalent degree of mechanical stress to stretch the lungs. Additionally, PEEP was set to zero, respiratory rate was 80 breaths per minute, and inspired gas was changed to 96% O_2/4% CO_2 to prevent hypocapnia. Animals were ventilated with this constant tidal volume for 60 min or until airway plateau pressure had increased by 15%, whichever occurred first. Ventilation was then returned to match the baseline “pre-stretch” strategy, and maintained for a further 3 hours. Sustained inflation maneuvers were performed every 30 min during this “non-injurious” ventilation period to reduce the development of atelectasis. Anesthesia was maintained by bolus intraperitoneal administration of ketamine:xylazine (40 mg/kg:4 mg/kg) every 20 to 25 min. Animals were terminated by overdose of anesthetic followed by exsanguination. The lungs were lavaged with 750 µl of ice-cold PBS containing phosphatase inhibitor cocktail (Calbiochem), and the recovered fluid

was centrifuged at 210*g* for 5 min at 4°C. Aliquots of supernatant and the lavage cell pellet were frozen at -80°C. After lavage, the chest wall was opened and the right lung was tied off at the hilum, removed, and snap-frozen in liquid N_2. Finally, the left lung was inflated with 4% paraformaldehyde at 20 cm H_2O before being embedded in paraffin for histological analysis.

Precision-cut lung slices

Mice were terminally anaesthetized as described earlier, exsanguinated, and then had their lungs and trachea exposed. The lungs were perfused with PBS containing heparin (200 U/ml) through the left ventricle to remove all of the blood. The trachea was cannulated and the lungs were filled with 1.2 ml of 1% low-melting point agarose pre-warmed to 42°C, which was followed by 0.3 ml of air. The lungs were cooled by covering them with ice-cold PBS to enable the agarose to set, carefully removed, and the lobes were dissected. Lung slices of 150-µm thickness were prepared from each lung lobe with a VT1200S Vibratome (Leica). Lung slices (2 per well) were cultured overnight in serum-free DMEM containing penicillin and streptomycin before being stimulated. To induce contraction of the lung slices, they were repeatedly stimulated for 10 min with 100 µM methacholine at one-hour intervals for 8 hours. After they were stimulated, the lung slices were washed in PBS and homogenized in protein lysis buffer [20 mM Tris-HCl (pH 7.4), 137 nM NaCl, 2 nM EDTA, 25 mM β-glycerophosphate, 1 nM Na_3VO_4, 1% Triton X-100, 10% glycerol]. This buffer was supplemented with leupeptin, phenylmethylsulfonyl fluoride (PMSF), protease inhibitor (protease inhibitor mixture, Roche Applied Science), dithiothreitol (DTT), and phosphatase inhibitor (PhosStop, Roche Applied Science) .

Western blotting

The amounts of $G\alpha_q$ or IL-33 in whole-cell extracts of ATII cells were determined by Western blotting analysis. Protein samples (30 μg per lane) were subjected to electrophoresis on a 10% SDS-polyacrylamide gel and blotted onto a polyvinylidene fluoride (PVDF) membrane. After blocking for 1 hour (in TBS, 5% nonfat milk, 0.1% Tween 20), the membrane was incubated either overnight at 4°C with monoclonal anti-$G\alpha_q$ antibody in blocking buffer or for 48 hours with anti-IL-33 antibody (Nessy-1). After being washed [with PBS (pH 7.4), 0.3% Tween-20] the membrane was incubated at room temperature in blocking buffer with the appropriate HRP-conjugated secondary antibody for 1 or 2 hours for the detection of $G\alpha_q$ or IL-33, respectively. The membrane was incubated with Enhanced Chemiluminescence (ECL) Western blotting detection reagent and visualized by exposure to Hyperfilm-ECL. To quantify the differential production of IL-33 in the alveolar epithelial cells, densitometry was performed with Adobe Photoshop CC2014 software and the mean pixel densities were calculated. Densitometry data are presented as the ratio of IL-33 abundance to that of GAPDH in cells independently isolated from three mice per group.

RNA isolation and quantitative RT-PCR

Total RNA was extracted from lung samples, purified ATII cells, and BAL cells by homogenization in Trizol B (Invitrogen) and was processed according to the manufacturer's instructions. Samples were reverse-transcribed into complementary DNA (cDNA) with Moloney murine leukemia virus reverse transcriptase (for BAL cell pellets; Promega, UK) or Superscript II reverse transcriptase (for lung samples and ATII cells; Invitrogen, UK). The cDNA was subjected to quantitative RT-PCR analysis with gene-specific primers (table S1). Amplification was performed with an MXPro3000 (Stratagene, UK) with KapaSybr FastTaq (Anachem, UK) on the following program: initial denaturation at 95°C for 3 min followed by 40 cycles of 95°C for 30 s, 60°C for 30 s, and 72°C for 10 s. Amplification of a single DNA

product was confirmed by melting curve analysis. Data were analyzed relative to the abundances of the housekeeping genes *hypoxanthine phosphoribosyltransferase 1 (Hprt)* (for BAL samples) or *glucuronidase beta (Gusb)* (for whole-lung and ATII samples) and expressed as the fold-change in mRNA abundance using the ΔΔCt equation as described previously (53).

Bronchoalveolar lavage and cytospin analysis

Animals were terminally anaesthetized as described earlier, their tracheae were cannulated, and their lungs were washed with eight sequential 0.5-ml aliquots of cold PBS or PBS containing 1x phosphatase inhibitor solution (ActivMotif, UK). Aliquots were pooled and centrifuged, and the cell pellets were resuspended in PBS or PBS containing 1x phosphatase inhibitor solution (ActivMotif) for the analysis of pSmad2 and macrophage culture experiments. Cells were counted with a Sceptre 2.0 automated cell counter (Millipore, UK) and cell concentrates were cytospun onto glass slides and stained with Diff-Quick (Dade Diagnostics). Cell subsets were counted under ×40 objective magnification (200 cells per slide). Designation of alveolar macrophages as “normal” or “enlarged” was made visually based on cell size. The enlarged macrophages observed only in *SftpC*$^{+/-}$;*Gnaq*$^{fl/fl}$;*Gna11*$^{-/-}$ mice were identified after cytospin analysis by their increased cytoplasmic surface area when compared with alveolar macrophages from *Gna11*$^{-/-}$, *Gna12*$^{-/-}$, or *SftpC*$^{+/-}$;*Gna12*$^{-/-}$;*Gna13*$^{fl/fl}$ animals.

Culture of BAL cells

BAL cells were collected into serum-free Dulbecco’s Modified Eagle Medium (DMEM, Lonza. UK) containing glutamine, penicillin, and streptomycin and pelleted by centrifugation at 150*g* for 5 min at 4°C. BAL fluid (BALF) was collected, and BAL cells were pooled from

Gna11$^{-/-}$ mice (n = 10 to 24 mice) and *SftpC*$^{+/-}$;*Gnaq*$^{fl/fl}$;*Gna11*$^{-/-}$ mice (n = 3 to 5). For crossover experiments in which the effect of secreted factors in BALF on gene expression were examined, 2.5 x 10^5 BAL cells from *Gna11*$^{-/-}$ mice or *SftpC*$^{+/-}$;*Gnaq*$^{fl/fl}$;*Gna11*$^{-/-}$ mice were resuspended in 1 ml of the appropriate BALF and then were plated into 12-well plates for RNA endpoint analysis or in 250 μl of BALF and then were plated into 8-well chamber slides for immunofluorescent staining. Cells were incubated with BALF for 24 hours at 37°C, non-adherent cells were removed by washing, and the adherent macrophages were lysed by the addition of Trizol B before RNA was isolated or were fixed in ice-cold 100% methanol for 10 min before immunofluorescent staining was performed. For cytokine stimulation or blocking experiments, serum-free DMEM or BALF was mixed with TGFβ (2 ng/ml), anti-TGFβ antibody (5 μg/ml, 1D11), or anti-IL-33 antibody (1.5 μg/ml, Bondy-1-1) and incubated with BAL cells in culture for 24 hours.

Immunostaining and image analysis

Formalin-fixed lung tissue sections (5-μm thickness) were de-paraffinized and re-hydrated before antigen retrieval by being microwaved in 10 mM citric acid buffer (pH 6.0). Endogenous peroxidase activity in the sections was blocked with methanol containing 3% H_2O_2 for 15 min at room temperature. Nonspecific binding was blocked with 5% normal serum before the sections were incubated overnight with primary antibody at 4°C, which was followed by a 30- to 60-min incubation with an appropriately labeled secondary antibody at room temperature. All sections were visualized with DAB and counterstained with hematoxylin and mounted in DPX (Sigma-Aldrich, UK) for immunohistochemical analysis or were counterstained with DAPI (Invitrogen, UK) for 5 min and mounted in Prolong Gold Antifade (Invitrogen) for immunofluorescence analysis. To stain isolated alveolar macrophages, methanol-fixed cells were permeabilized with 0.1% triton X-100 for 10 min

before being blocked in 5% normal serum, incubated overnight with primary antibody at 4°C, and then incubated for 30 to 60 min with an appropriately fluorescently labeled secondary antibody at room temperature. All antibody incubations were performed in staining buffer containing PBS, 5% serum, and 0.1% BSA. Slides were washed in PBS (Sigma-Aldrich). Images were captured with a Nikon 90i (for immunohistochemistry) or a Nikon Ti confocal microscope (for immunofluorescence) with NIS-Elements Software v3.2. To quantify the staining of isolated alveolar macrophages, individual cells were identified with NIS-Elements Software v3.2, and the total numbers of pixels for both antibody-stained and negative control cells were calculated. Pixel counts were determined in 40 to 100 individual cells from images captured in 5 to 20 randomly selected fields of view. The average number of pixels per cell in the unstained sections (negative control) were subtracted from the values calculated for antibody-stained sections to eliminate autofluorescence, and the data were presented as the number of pixels/cell.

Isolation of type II alveolar epithelial cells

Mice were terminally anaesthetized as described earlier, exsanguinated, and had their lungs and trachea exposed. The lungs were perfused with PBS containing heparin (200 U/ml) through the left ventricle to remove all of the blood. The trachea was cannulated and bronchoalveolar lavage was performed with eight sequential 0.5-ml aliquots of cold PBS to remove leukocytes. The lungs were filled with 1 ml Dispase (BD Pharmingen, UK) and allowed to collapse naturally before the instillation of 0.5 ml of 1% low melting point agarose (Promega) pre-warmed to 42°C. The lungs were then covered in ice for 2 min to enable the agarose to set before they were removed. The lungs were incubated at room temperature for 45 min in 2 ml of Dispase and then washed briefly in ice-cold PBS before being transferred to petri dishes containing DMEM with 10% FCS, glutamine, and DNase 1(100 U/ml, Sigma).

Lung tissue was carefully separated from the large airways and blood vessels before the cell suspension was dissociated. The crude cell suspension was sequentially filtered through 70- and 40-μm tissue sieves (BD) and then plated into plastic petri dishes coated with mouse IgG (1.5 mg IgG/plate). Nonadherent cells were collected after a 1-hour incubation at 37°C and were pelleted by centrifugation at 150*g* for 5 min. Contaminating leukocytes were removed by negative sorting with magnetic beads labeled with sheep anti-rat CD16/32 and CD45 antibodies (Dynabeads, Dynal) for 1 hour at 4°C according to the manufacturer's instructions. The remaining cells were resuspended in Bronchial Epithelial Growth Medium (BEGM; Lonza) without hydrocortisone and containing keratinocyte growth factor (10 μg/ml, R&D Systems) and the purity of the ATII cell suspension was assessed by modified Papanicolaou staining of cell cytospins as previously described (54). The cells were plated onto collagen-coated, 24-well plates and ATII cells were grown to confluence. Cell purity was routinely >75%, with the major contaminating cells being fibroblasts. For experiments in which ATII cells were to be used for mRNA analysis, an additional purification step was added after the completion of the standard protocol in which epithelial cells in the cell suspension were enriched by positive sorting with sheep anti-rat magnetic beads labeled with an anti-E-cadherin antibody (Dynabeads, Dynal). After washing to remove the bead-free cells, the mixture of beads and ATII cells was immediately mixed with Trizol B reagent.

ELISA/Luminex analysis

Total TGFβ1 concentrations in murine lung homogenates were measured after acid-activation of samples with a murine TGFβ1 Quantikine ELISA kit (R&D Systems). Concentrations of active TGFβ secreted into lung slice supernatants were also determined with this ELISA kit, but without acid activation. The concentrations of soluble ST2 were measured in lung homogenates and BALF with a mouse ST2/IL-1 R4 Quantikine ELISA Kit (R&D Systems),

whereas the concentrations of IL-33, IL-4, IL-10, and IL-13 were assessed with a customized mouse Magnetic Luminex Screening Assay (R&D Systems). Additional IL-33 analysis was performed with a mouse IL-33 ELISA kit (R&D Systems). All assays were performed according to the manufacturers' instructions.

Measurement of pSmad2 by ELISA

Nuclear protein was prepared from BAL cells with a Nuclear Extract kit (ActivMotif) according to the manufacturer's protocol. To analyze lung slices, total protein extracts were generated according to the manufacturer's instructions (Cell Signalling Technologies, UK). The amounts of pSmad2 were measured in 10 µg of nuclear protein (BAL cells) or 10 µg of total protein (lung slices) with a solid-phase Pathscan PhosphoSmad2 ($Ser^{465/467}$) sandwich ELISA kit (Cell Signalling Technologies, UK) according to the manufacturer's instructions.

Microarray analysis

Total RNA was assessed quantitatively on a Nanodrop and qualitatively (RIN>7) by Bioanalyser (Agilent, UK). After the quantity and quality of RNA were assessed, 10 ng of total RNA was used to prepare microarray hybridization probes with Epistem's RNAamp RNA amplification kits (Epistem, Manchester, UK). After fragmentation the biotinylated cRNA was hybridized to Genechip Murine MOE430 2.0 microarrays (Epistem). After hybridization, the microarrays were washed and scanned with Genechip Scanner 7G. Microarray data were background-corrected, Log_2-transformed, and normalized with Robust Multi-array Average (RMA), followed by quantile normalization, and the RMA data from all of the arrays that passed quality control were analyzed with Partek Genomics Suite version 6.5. Principle Component Analysis (PCA) was used to interrogate the effects of all of the tracked and recorded experimental technical factors (dates, yields, randomization order, etc.)

on overall cohort data structure. Multivariate analysis of variance (ANOVA) was applied within Partek GS software for each pairwise comparison of groups using the Method of Moments. To further rank or prioritize genes that might be useful as candidate biomarkers, the degree of change in RNA abundance, or fold change, was used to select genes that differed in expression statistically significantly by one-way ANOVA (unadjusted *P* value of < 0.05) between compared groups and also exhibited a two-fold or greater change in expression. Further selection was performed by establishing overlaps between treatment groups. Further investigation of biological relevance was performed with Ingenuity IPA software.

Statistical analysis

All statistical analyses were performed with GraphPad Prism 6 software. Data were assessed for normality. Where differences between two groups were measured, the pooled mean values were compared with unpaired *t* tests. Comparisons between more than two groups were made by one-way ANOVA with Bonferroni or Dunn-Šidák multiple testing corrections applied to post-hoc, pairwise comparisons. Comparisons between groups over multiple time points were made by repeated measures ANOVA. Corrected *P* values < 0.05 were considered to be statistically significant.

Supplementary materials

Fig. S1 Characterization of alveolar epithelial cell–specific, G protein–deficient mouse colonies.
Fig. S2 Histological analysis of littermate control mice.
Fig. S3. Loss of epithelial $G\alpha_q/G\alpha_{11}$ signaling leads to altered lung function.
Fig. S4 Effect of the deficiency in epithelial Gq/11 signaling on the concentrations of T_H2 cytokines and ST2 in the lung.
Table S1. Sequences of genotyping primers.
Table S2. Sequences of RT-PCR primers.
Data file S1. Affymetrix gene array data.

References and Notes

1. Worzfeld, T., N. Wettschureck, and S. Offermanns. 2008. G(12)/G(13)-mediated signalling in mammalian physiology and disease. *Trends Pharmacol Sci* 29: 582-589.
2. Sanchez-Fernandez, G., S. Cabezudo, C. Garcia-Hoz, C. Beninca, A. M. Aragay, F. Mayor, Jr., and C. Ribas. 2014. Galphaq signalling: the new and the old. *Cell Signal* 26: 833-848.
3. Geng, H., R. Lan, P. K. Singha, A. Gilchrist, P. H. Weinreb, S. M. Violette, J. M. Weinberg, P. Saikumar, and M. A. Venkatachalam. 2012. Lysophosphatidic acid increases proximal tubule cell secretion of profibrotic cytokines PDGF-B and CTGF through LPA2- and Galphaq-mediated Rho and alphavbeta6 integrin-dependent activation of TGF-beta. *Am J Pathol* 181: 1236-1249.
4. Xu, M. Y., J. Porte, A. J. Knox, P. H. Weinreb, T. M. Maher, S. M. Violette, R. J. McAnulty, D. Sheppard, and G. Jenkins. 2009. Lysophosphatidic acid induces alphavbeta6 integrin-mediated TGF-beta activation via the LPA2 receptor and the small G protein G alpha(q). *Am J Pathol* 174: 1264-1279.
5. Bonniaud, P., M. Kolb, T. Galt, J. Robertson, C. Robbins, M. Stampfli, C. Lavery, P. J. Margetts, A. B. Roberts, and J. Gauldie. 2004. Smad3 null mice develop airspace enlargement and are resistant to TGF-beta-mediated pulmonary fibrosis. *J Immunol* 173: 2099-2108.
6. Li, M., M. S. Krishnaveni, C. Li, B. Zhou, Y. Xing, A. Banfalvi, A. Li, V. Lombardi, O. Akbari, Z. Borok, and P. Minoo. 2011. Epithelium-specific deletion of TGF-beta receptor type II protects mice from bleomycin-induced pulmonary fibrosis. *J Clin Invest* 121: 277-287.
7. Sime, P. J., Z. Xing, F. L. Graham, K. G. Csaky, and J. Gauldie. 1997. Adenovector-mediated gene transfer of active transforming growth factor-beta1 induces prolonged severe fibrosis in rat lung. *J Clin Invest* 100: 768-776.
8. Pittet, J. F., M. J. Griffiths, T. Geiser, N. Kaminski, S. L. Dalton, X. Huang, L. A. Brown, P. J. Gotwals, V. E. Koteliansky, M. A. Matthay, and D. Sheppard. 2001. TGF-beta is a critical mediator of acute lung injury. *J Clin Invest* 107: 1537-1544.
9. Jenkins, R. G., X. Su, G. Su, C. J. Scotton, E. Camerer, G. J. Laurent, G. E. Davis, R. C. Chambers, M. A. Matthay, and D. Sheppard. 2006. Ligation of protease-activated receptor 1 enhances alpha(v)beta6 integrin-dependent TGF-beta activation and promotes acute lung injury. *J Clin Invest* 116: 1606-1614.
10. Hersh, C. P., N. N. Hansel, K. C. Barnes, D. A. Lomas, S. G. Pillai, H. O. Coxson, R. A. Mathias, N. M. Rafaels, R. A. Wise, J. E. Connett, B. J. Klanderman, F. L. Jacobson, R. Gill, A. A. Litonjua, D. Sparrow, J. J. Reilly, and E. K. Silverman. 2009. Transforming growth factor-beta receptor-3 is associated with pulmonary emphysema. *Am J Respir Cell Mol Biol* 41: 324-331.
11. Celedon, J. C., C. Lange, B. A. Raby, A. A. Litonjua, L. J. Palmer, D. L. DeMeo, J. J. Reilly, D. J. Kwiatkowski, H. A. Chapman, N. Laird, J. S. Sylvia, M. Hernandez, F. E. Speizer, S. T. Weiss, and E. K. Silverman. 2004. The transforming growth factor-beta1 (TGFB1) gene is associated with chronic obstructive pulmonary disease (COPD). *Hum Mol Genet* 13: 1649-1656.
12. Wu, L., J. Chau, R. P. Young, V. Pokorny, G. D. Mills, R. Hopkins, L. McLean, and P. N. Black. 2004. Transforming growth factor-beta1 genotype and susceptibility to chronic obstructive pulmonary disease. *Thorax* 59: 126-129.
13. Tatler, A. L., and G. Jenkins. 2012. TGF-beta activation and lung fibrosis. *Proc Am Thorac Soc* 9: 130-136.

14. Karsdal, M. A., L. Larsen, M. T. Engsig, H. Lou, M. Ferreras, A. Lochter, J. M. Delaisse, and N. T. Foged. 2002. Matrix metalloproteinase-dependent activation of latent transforming growth factor-beta controls the conversion of osteoblasts into osteocytes by blocking osteoblast apoptosis. *J Biol Chem* 277: 44061-44067.
15. Taipale, J., K. Koli, and J. Keski-Oja. 1992. Release of transforming growth factor-beta 1 from the pericellular matrix of cultured fibroblasts and fibrosarcoma cells by plasmin and thrombin. *J Biol Chem* 267: 25378-25384.
16. Tatler, A. L., J. Porte, A. Knox, G. Jenkins, and L. Pang. 2008. Tryptase activates TGFbeta in human airway smooth muscle cells via direct proteolysis. *Biochem Biophys Res Commun* 370: 239-242.
17. Mu, D., S. Cambier, L. Fjellbirkeland, J. L. Baron, J. S. Munger, H. Kawakatsu, D. Sheppard, V. C. Broaddus, and S. L. Nishimura. 2002. The integrin alpha(v)beta8 mediates epithelial homeostasis through MT1-MMP-dependent activation of TGF-beta1. *J Cell Biol* 157: 493-507.
18. Munger, J. S., X. Huang, H. Kawakatsu, M. J. Griffiths, S. L. Dalton, J. Wu, J. F. Pittet, N. Kaminski, C. Garat, M. A. Matthay, D. B. Rifkin, and D. Sheppard. 1999. The integrin alpha v beta 6 binds and activates latent TGF beta 1: a mechanism for regulating pulmonary inflammation and fibrosis. *Cell* 96: 319-328.
19. Tatler, A. L., A. E. John, L. Jolly, A. Habgood, J. Porte, C. Brightling, A. J. Knox, L. Pang, D. Sheppard, X. Huang, and G. Jenkins. 2011. Integrin alphavbeta5-mediated TGF-beta activation by airway smooth muscle cells in asthma. *J Immunol* 187: 6094-6107.
20. Yang, Z., Z. Mu, B. Dabovic, V. Jurukovski, D. Yu, J. Sung, X. Xiong, and J. S. Munger. 2007. Absence of integrin-mediated TGFbeta1 activation in vivo recapitulates the phenotype of TGFbeta1-null mice. *J Cell Biol* 176: 787-793.
21. Aluwihare, P., Z. Mu, Z. Zhao, D. Yu, P. H. Weinreb, G. S. Horan, S. M. Violette, and J. S. Munger. 2009. Mice that lack activity of alphavbeta6- and alphavbeta8-integrins reproduce the abnormalities of Tgfb1- and Tgfb3-null mice. *J Cell Sci* 122: 227-232.
22. Morris, D. G., X. Huang, N. Kaminski, Y. Wang, S. D. Shapiro, G. Dolganov, A. Glick, and D. Sheppard. 2003. Loss of integrin alpha(v)beta6-mediated TGF-beta activation causes Mmp12-dependent emphysema. *Nature* 422: 169-173.
23. Offermanns, S., L. P. Zhao, A. Gohla, I. Sarosi, M. I. Simon, and T. M. Wilkie. 1998. Embryonic cardiomyocyte hypoplasia and craniofacial defects in G alpha q/G alpha 11-mutant mice. *EMBO J* 17: 4304-4312.
24. Gu, J. L., S. Muller, V. Mancino, S. Offermanns, and M. I. Simon. 2002. Interaction of G alpha(12) with G alpha(13) and G alpha(q) signaling pathways. *Proc Natl Acad Sci U S A* 99: 9352-9357.
25. Offermanns, S., V. Mancino, J. P. Revel, and M. I. Simon. 1997. Vascular system defects and impaired cell chemokinesis as a result of Galpha13 deficiency. *Science* 275: 533-536.
26. Offermanns, S., C. F. Toombs, Y. H. Hu, and M. I. Simon. 1997. Defective platelet activation in G alpha(q)-deficient mice. *Nature* 389: 183-186.
27. Offermanns, S., K. Hashimoto, M. Watanabe, W. Sun, H. Kurihara, R. F. Thompson, Y. Inoue, M. Kano, and M. I. Simon. 1997. Impaired motor coordination and persistent multiple climbing fiber innervation of cerebellar Purkinje cells in mice lacking Galphaq. *Proc Natl Acad Sci U S A* 94: 14089-14094.

28. Hartmann, J., R. Blum, Y. Kovalchuk, H. Adelsberger, R. Kuner, G. M. Durand, M. Miyata, M. Kano, S. Offermanns, and A. Konnerth. 2004. Distinct roles of Galpha(q) and Galpha11 for Purkinje cell signaling and motor behavior. *J Neurosci* 24: 5119-5130.
29. Offermanns, S., E. Heiler, K. Spicher, and G. Schultz. 1994. Gq and G11 are concurrently activated by bombesin and vasopressin in Swiss 3T3 cells. *FEBS Lett* 349: 201-204.
30. Wange, R. L., A. V. Smrcka, P. C. Sternweis, and J. H. Exton. 1991. Photoaffinity labeling of two rat liver plasma membrane proteins with [32P]gamma-azidoanilido GTP in response to vasopressin. Immunologic identification as alpha subunits of the Gq class of G proteins. *J Biol Chem* 266: 11409-11412.
31. Wu, D., A. Katz, C. H. Lee, and M. I. Simon. 1992. Activation of phospholipase C by alpha 1-adrenergic receptors is mediated by the alpha subunits of Gq family. *J Biol Chem* 267: 25798-25802.
32. Xu, X., J. T. Croy, W. Zeng, L. Zhao, I. Davignon, S. Popov, K. Yu, H. Jiang, S. Offermanns, S. Muallem, and T. M. Wilkie. 1998. Promiscuous coupling of receptors to Gq class alpha subunits and effector proteins in pancreatic and submandibular gland cells. *J Biol Chem* 273: 27275-27279.
33. Hepler, J. R., T. Kozasa, A. V. Smrcka, M. I. Simon, S. G. Rhee, P. C. Sternweis, and A. G. Gilman. 1993. Purification from Sf9 cells and characterization of recombinant Gq alpha and G11 alpha. Activation of purified phospholipase C isozymes by G alpha subunits. *J Biol Chem* 268: 14367-14375.
34. Rhee, S. G. 2001. Regulation of phosphoinositide-specific phospholipase C. *Annu Rev Biochem* 70: 281-312.
35. Juncadella, I. J., A. Kadl, A. K. Sharma, Y. M. Shim, A. Hochreiter-Hufford, L. Borish, and K. S. Ravichandran. 2013. Apoptotic cell clearance by bronchial epithelial cells critically influences airway inflammation. *Nature* 493: 547-551.
36. Grainger, J. R., K. A. Smith, J. P. Hewitson, H. J. McSorley, Y. Harcus, K. J. Filbey, C. A. Finney, E. J. Greenwood, D. P. Knox, M. S. Wilson, Y. Belkaid, A. Y. Rudensky, and R. M. Maizels. 2010. Helminth secretions induce de novo T cell Foxp3 expression and regulatory function through the TGF-beta pathway. *J Exp Med* 207: 2331-2341.
37. McSorley, H. J., N. F. Blair, K. A. Smith, A. N. McKenzie, and R. M. Maizels. 2014. Blockade of IL-33 release and suppression of type 2 innate lymphoid cell responses by helminth secreted products in airway allergy. *Mucosal Immunol* 7: 1068-1078.
38. Huang, X. Z., J. F. Wu, D. Cass, D. J. Erle, D. Corry, S. G. Young, R. V. Farese, Jr., and D. Sheppard. 1996. Inactivation of the integrin beta 6 subunit gene reveals a role of epithelial integrins in regulating inflammation in the lung and skin. *J Cell Biol* 133: 921-928.
39. Kukkonen, M. K., E. Tiili, T. Vehmas, P. Oksa, P. Piirila, and A. Hirvonen. 2013. Association of genes of protease-antiprotease balance pathway to lung function and emphysema subtypes. *BMC Pulm Med* 13: 36.
40. Zhiguang, X., C. Wei, R. Steven, D. Wei, Z. Wei, M. Rong, L. Zhanguo, and Z. Lianfeng. 2010. Over-expression of IL-33 leads to spontaneous pulmonary inflammation in mIL-33 transgenic mice. *Immunol Lett* 131: 159-165.
41. Kurowska-Stolarska, M., B. Stolarski, P. Kewin, G. Murphy, C. J. Corrigan, S. Ying, N. Pitman, A. Mirchandani, B. Rana, N. van Rooijen, M. Shepherd, C. McSharry, I. B. McInnes, D. Xu, and F. Y. Liew. 2009. IL-33 amplifies the polarization of alternatively activated macrophages that contribute to airway inflammation. *J Immunol* 183: 6469-6477.

42. Li, D., R. Guabiraba, A. G. Besnard, M. Komai-Koma, M. S. Jabir, L. Zhang, G. J. Graham, M. Kurowska-Stolarska, F. Y. Liew, C. McSharry, and D. Xu. 2014. IL-33 promotes ST2-dependent lung fibrosis by the induction of alternatively activated macrophages and innate lymphoid cells in mice. *J Allergy Clin Immunol*.
43. Byers, D. E., J. Alexander-Brett, A. C. Patel, E. Agapov, G. Dang-Vu, X. Jin, K. Wu, Y. You, Y. Alevy, J. P. Girard, T. S. Stappenbeck, G. A. Patterson, R. A. Pierce, S. L. Brody, and M. J. Holtzman. 2013. Long-term IL-33-producing epithelial progenitor cells in chronic obstructive lung disease. *J Clin Invest* 123: 3967-3982.
44. Giacomini, M. M., M. A. Travis, M. Kudo, and D. Sheppard. 2012. Epithelial cells utilize cortical actin/myosin to activate latent TGF-beta through integrin alpha(v)beta(6)-dependent physical force. *Exp Cell Res* 318: 716-722.
45. Shi, M., J. Zhu, R. Wang, X. Chen, L. Mi, T. Walz, and T. A. Springer. 2011. Latent TGF-beta structure and activation. *Nature* 474: 343-349.
46. Sheppard, D., D. S. Cohen, A. Wang, and M. Busk. 1992. Transforming growth factor beta differentially regulates expression of integrin subunits in guinea pig airway epithelial cells. *J Biol Chem* 267: 17409-17414.
47. Araya, J., S. Cambier, J. A. Markovics, P. Wolters, D. Jablons, A. Hill, W. Finkbeiner, K. Jones, V. C. Broaddus, D. Sheppard, A. Barzcak, Y. Xiao, D. J. Erle, and S. L. Nishimura. 2007. Squamous metaplasia amplifies pathologic epithelial-mesenchymal interactions in COPD patients. *J Clin Invest* 117: 3551-3562.
48. Kakkar, R., H. Hei, S. Dobner, and R. T. Lee. 2012. Interleukin 33 as a mechanically responsive cytokine secreted by living cells. *J Biol Chem* 287: 6941-6948.
49. Rani, R., A. G. Smulian, D. R. Greaves, S. P. Hogan, and D. R. Herbert. 2011. TGF-beta limits IL-33 production and promotes the resolution of colitis through regulation of macrophage function. *Eur J Immunol* 41: 2000-2009.
50. Okubo, T., P. S. Knoepfler, R. N. Eisenman, and B. L. Hogan. 2005. Nmyc plays an essential role during lung development as a dosage-sensitive regulator of progenitor cell proliferation and differentiation. *Development* 132: 1363-1374.
51. Dunnill, M. S. 1962. Quantitative Methods in the Study of Pulmonary Pathology *Thorax* 17: 320-328.
52. Wilson, M. R., B. V. Patel, and M. Takata. 2012. Ventilation with "clinically relevant" high tidal volumes does not promote stretch-induced injury in the lungs of healthy mice. *Crit Care Med* 40: 2850-2857.
53. Weglarz, L., I. Molin, A. Orchel, B. Parfiniewicz, and Z. Dzierzewicz. 2006. Quantitative analysis of the level of p53 and p21(WAF1) mRNA in human colon cancer HT-29 cells treated with inositol hexaphosphate. *Acta Biochim Pol* 53: 349-356.
54. Dobbs, L. G. 1990. Isolation and culture of alveolar type II cells. *Am J Physiol* 258: L134-147.

Acknowledgments: We are grateful to B. Hogan (Duke University) for providing the Surfactant Protein C promoter (*SftpC*-Cre) mice used in these studies. **Funding:** This work was supported by the Wellcome Trust (project grant number 085350) and MRC MICA grant (G0901226). A.L.T. was supported by an NC3Rs David Sainsbury Fellowship (NC/K500501/1). **Author contributions:** A.E.J. generated and performed extensive characterization of the epithelial cell–specific G protein knockout mice, conceived and performed all of the lung function experiments in vitro and in vivo, performed all data analysis, and wrote and prepared the manuscript; M.W. and M.T. conceived of and performed the in vivo VILI experiments and provided critical analysis of the data; A.H. and J.P.

genotyped mouse colonies and performed immunohistological analysis of lung samples; A.L.T. and A.S. performed Western blotting analysis; G.M. performed Affymetrix gene array analysis; L.J. helped with in vivo lung function experiments; A.K. contributed to experimental design and data analysis and provided critical analysis of the manuscript' S.O. generated G protein knockout mice and provided critical analysis of manuscript' R.G.J. conceived of and oversaw the entire project, and wrote and prepared the manuscript. **Competing interests:** R.G.J. has Sponsored Research Agreements with GlaxoSmithKline, Novartis, and Biogen and performed consultancy for InterMune, MedImmune, Boehringer Ingelheim, Biogen, PharmAkea, Pulmatrix, and Roche, and received speaker fees from Boehringer Ingelheim, MedImmune, and Roche. All other authors have declared that they have no competing interests. **Data and materials availability:** The gene array data have been deposited to the Gene Expression Omnibus with the dataset identifier XXX.

Fig. 1. Age-related morphological changes in the lungs of mice with homozygous deficiency in $G\alpha_q$ and $G\alpha_{11}$ in alveolar epithelial cells. (**A**) Hematoxylin and eosin (H&E) staining of lung sections of *SftpC*$^{+/-}$;*Gnaq*$^{fl/fl}$;*Gna11*$^{-/-}$ mice at 2 to 24 weeks of age. Images are representative of three to ten mice/genotype. (**B**) Mean linear intercept analysis of airspace size in *Gna11*$^{-/-}$ mice (hatched bars) and *SftpC*$^{+/-}$;*Gnaq*$^{fl/fl}$;*Gna11*$^{-/-}$ mice (solid bars). Data are means ± SEM of three to ten mice/group. (**C**) FEV100/FVC was measured by invasive plethysmography of the indicated mice at 8 weeks of age. Data are means ± SEM of six mice/group. (**D** to **F**) The relative abundances of *Mmp2* mRNA (D), *Mmp9* mRNA (E), and *Mmp12* mRNA (F) in BAL leukocytes from 6- to 8-week-old *Gna11*$^{-/-}$ (n = 3) and *SftpC*$^{+/-}$;*Gnaq*$^{fl/fl}$;*Gna11*$^{-/-}$ (n = 6) mice were determined by RT-PCR analysis. *P < 0.05; **P < 0.01; ***P < 0.001 ; ****P < 0.0001 by one-way ANOVA with Bonferroni corrected post-hoc comparisons (B) or by unpaired *t* test (C to F). Scale bars, 100 μm.

Fig. 2. Decreased TGFβ activation after disruption of the Gq/G11 signaling pathway in alveolar epithelial cells. (**A**) Total TGFβ concentrations in lung homogenates from the indicated mice were measured by ELISA Data are from 10 mice/group and means are represented by horizontal bars. Each symbol represents an individual mouse. (**B**) Concentrations of spontaneously active TGFβ in supernatants from lung slices of the

indicated mice that were left unstimulated or were stimulated by repeated administration of 100 μM methacholine. Data are means ± SEM of three mice/group. (**C**) Lung slices from the indicated mice were left untreated or were stimulated repeatedly with 100 μM methacholine. The amounts of pSmad2 in the lung slices were measured by ELISA. Data are means ± SEM of four mice/group. (**D**) BAL cells from the indicated mice were cultured in the presence or absence of TGFβ (2 ng/ml) for 1 hour before the concentrations of pSmad2 in the cells were determined. Data are means ± SEM of four mice/group. (**E** and **F**) The relative abundances of *Itgb6* mRNA (E) and *Tsp1* mRNA (F) in ATII cells from *Gna11*$^{-/-}$ mice (n = 3) and *SftpC*$^{+/-}$*;Gnaq*$^{fl/fl}$*;Gna11*$^{-/-}$ mice (n = 3) were determined by RT-PCR analysis. The abundances of the indicated mRNAs were normalized to that of *Gusb* mRNA. Data are means ± SEM. **P* < 0.05; ***P* < 0.01; ****P* < 0.001 when analyzed by unpaired *t* test (A, E, and F) or one-way ANOVA with Dunn-Šidák corrected post-hoc comparisons (B to D).

Fig. 3. Aberrant responses in alveolar macrophages from *SftpC*$^{+/-}$*;Gnaq*$^{fl/fl}$*;Gna11*$^{-/-}$ mice. (**A**) The relative abundances of *Tgfbr1* and *Tgfbr2* mRNAs in BAL leukocytes from *Gna11*$^{-/-}$ and *SftpC*$^{+/-}$*;Gnaq*$^{fl/fl}$*;Gna11*$^{-/-}$ mice were determined by RT-PCR analysis. Data are means ± SEM of six mice per group. (**B**) The relative abundance of *Tgfbr1* mRNA in alveolar macrophages from *SftpC*$^{+/-}$*;Gnaq*$^{fl/fl}$*;Gna11*$^{-/-}$ mice cultured for 24 hours in BALF from *SftpC*$^{+/-}$*;Gnaq*$^{fl/fl}$*;Gna11*$^{-/-}$ mice or from *Gna11*$^{-/-}$ mice in the presence or absence of an anti-TGFβ antibody (α-TGFβ, 5 μg/ml). Data are means ± SEM and combined from three independent experiments with cells, BALF, or both pooled from 10 to 24 *Gna11*$^{-/-}$ mice per experiment or three to five *SftpC*$^{+/-}$*;Gnaq*$^{fl/fl}$*;Gna11*$^{-/-}$ mice per experiment. (**C**) The relative abundances of *Tgfbr1* and *Tgfbr2* mRNA in alveolar macrophages from *SftpC*$^{+/-}$*;Gnaq*$^{fl/fl}$*;Gna11*$^{-/-}$ mice that were left unstimulated or were stimulated with TGFβ (2 ng/ml) for 8 hours were determined by RT-PCR. Data are means ± SEM of six mice per group. (**D**

and **E**) The relative abundances of *Mmp12* mRNA in alveolar macrophages isolated from *Gna11*$^{-/-}$ mice and cultured for 24 hours in BALF from *Gna11*$^{-/-}$ mice or *SftpC*$^{+/-}$*;Gnaq*$^{fl/fl}$*;Gna11*$^{-/-}$ mice in the presence or absence of (D) TGFβ (2 ng/ml) or (E) anti-TGFβ antibody (5 μg/ml) were determined by RT-PCR. Data are combined from four independent experiments with cells, BALF, or both pooled from 10 to 24 *Gna11*$^{-/-}$ mice per experiment or three to five *SftpC*$^{+/-}$*;Gnaq*$^{fl/fl}$*;Gna11*$^{-/-}$ mice per experiment. The abundances of the indicated mRNAs were normalized to that of *Hprt* mRNA. Data are means ± SEM. **P* < 0.05; ***P* < 0.01; ****P* < 0.001 when analyzed by unpaired *t* test (A) or one-way ANOVA with Dunn-Šidák corrected post-hoc comparisons (B to D).

Fig. 4. Accumulation of M2 macrophages in the lungs of mice with Gαq/Gα11-deficient alveolar epithelial cells. (**A**) High-power magnified image of enlarged and vacuolated cells (marked with arrows) in the alveoli of *SftpC*$^{+/-}$*;Gnaq*$^{fl/fl}$*;Gna11*$^{-/-}$mice. Images are representative of three experiments. (**B**) Immunofluorescent staining of F4/80-positive cells (marked with arrows) in the lungs of *SftpC*$^{+/-}$*;Gnaq*$^{fl/fl}$*;Gna11*$^{-/-}$ mice. Images are representative of three experiments. (**C**) Total cell counts in BALF isolated from the indicated mice. (**D**) Cytospin analysis of BAL leukocyte populations isolated from the indicated mice and stained with Diff-Quik. (**E**) Analysis of alveolar macrophage morphology. The percentages of normal and enlarged macrophages in the BALF of the indicated mice were calculated. (**F** and **G**) Immunofluorescence staining (left) and quantification of M2 markers (right; number of pixels/cell) in BAL cells from *Gna11*$^{-/-}$ and *SftpC*$^{+/-}$*;Gnaq*$^{fl/fl}$*;Gna11*$^{-/-}$ mice for (F) RELMα, mannose receptor, Sphk1, and iNOS and (G) IL-10. Data in (C) and (E) are means ± SEM of three to ten mice per genotype. Data in (F) and (G) are means + SEM of the pixel counts/cell from 30 to 80 individual cells pooled from two independent experiments. **P* < 0.05; ***P* < 0.01; ****P* < 0.001; *****P* < 0.0001 when

analyzed by one-way ANOVA with Bonferroni corrected post-hoc comparisons (C) or by unpaired *t* test (E). All experiments were performed with 6-week-old mice. Scale bars, 20 μm.

Fig. 5. Increased alveolar IL-33 production in the absence of Gq/11 signaling. (**A**) Hierarchical cluster analysis of differentially expressed genes in epithelial cells from *SftpC*$^{+/-}$;*Gnaq*$^{fl/fl}$;*Gna11*$^{-/-}$, *Gna11*$^{-/-}$, *Gna12*$^{-/-}$, and *SftpC*$^{+/-}$;*Gna13*$^{fl/fl}$;*Gna12*$^{-/-}$ mice (n = 3 mice/genotype). (**B**) Top: Alveolar epithelial cells from the indicated mice were analyzed by Western blotting with antibodies against the indicated proteins. Bottom: Densitometric analysis of the relative abundance of IL-33 protein normalized to that of GAPDH. Data are means ± SEM of three mice/genotype. (**C** and **D**) Low-power (C) and high-power (D) magnified images of immunohistochemical staining for IL-33 in the lungs of *Gna11*$^{-/-}$ and *SftpC*$^{+/-}$;*Gnaq*$^{fl/fl}$/*Gna11*$^{-/-}$ mice. Images are representative of three mice/genotype. (**E**) The amounts of IL-33 in lung homogenates from *Gna11*$^{-/-}$ and *SftpC*$^{+/-}$;*Gnaq*$^{fl/fl}$;*Gna11*$^{-/-}$ mice were determined by ELISA. Data are from 11 mice/genotype and means are presented by horizontal bars. (**F**) ST2 concentrations in BALF from *Gna11*$^{-/-}$ mice and *SftpC*$^{+/-}$;*Gnaq*$^{fl/fl}$/*Gna11*$^{-/-}$ mice were determined by ELISA Data are from 8 mice/genotype and means are presented by horizontal bars. (**G**) The concentrations of IL-33 in lung homogenates from *Itgb6*$^{-/-}$ mice and their wild-type (WT) littermate controls were determined by ELISA. Data are from 5 or 6 mice/genotype and means are presented by horizontal bars. **P* < 0.05; ***P* < 0.01; ****P* < 0.001 by unpaired *t* test. Scale bars, 20 μm (C) and 10 μm (D).

Fig 6. Regulation of alveolar macrophage M2 phenotype by IL-33. (**A** and **B**) The relative abundances of *Il10* (A) and *Arg1* and *Sphk1* (B) mRNAs in alveolar macrophages that were isolated from *SftpC*$^{+/-}$;*Gnaq*$^{fl/fl}$;*Gna11*$^{-/-}$ mice and cultured for 24 hours in BALF from either

Gna11$^{-/-}$ mice or *SftpC*$^{+/-}$;*Gnaq*$^{fl/fl}$;*Gna11*$^{-/-}$ mice in the presence or absence of TGFβ (2 pg/ml) or anti–IL-33 blocking antibody (1.5 μg/ml). Data are combined from three independent experiments with cells pooled from 10 to 24 *Gna11*$^{-/-}$ mice and 3 to 5 *SftpC*$^{+/-}$;*Gnaq*$^{fl/fl}$;*Gna11*$^{-/-}$ mice per experiment. (**C** and **D**) Immunofluorescence analysis (C) and quantification (D) of RELMα abundance in alveolar macrophages isolated from *Gna11*$^{-/-}$ mice and cultured for 24 hours in BALF from *SftpC*$^{+/-}$;*Gnaq*$^{fl/fl}$;*Gna11*$^{-/-}$ mice in the presence or absence of anti-IL-33 blocking antibody (1.5 μg/ml). Data are combined from two independent experiments with cells pooled from 10 to 24 *Gna11*$^{-/-}$ mice and BALF isolated from 3 to 5 *SftpC*$^{+/-}$;*Gnaq*$^{fl/fl}$;*Gna11*$^{-/-}$ mice/experiment. Quantification was performed on 40 to 100 cells per treatment group in images captured from 5 to 20 fields of view. *$P < 0.05$; ****$P < 0.0001$ by one-way ANOVA with Dunn-Šidák corrected post-hoc comparisons (A) or by unpaired *t* test (D). Scale bars, 20 μm.

Fig. 7. Gq/11-dependent signaling pathways regulate stretch-mediated TGFβ production in the lungs. (**A** and **B**) Changes in peak inspiratory pressure (A) and plateau pressure (B) during the high-stretch (1 hour) and normal (low) ventilation periods (3 hours) in *Gna11*$^{-/-}$ and *SftpC*$^{+/-}$;*Gnaq*$^{fl/fl}$;*Gna11*$^{-/-}$ mice. (**C** and **D**) Effects of high stretch for 1 hour on lung elastance (C) and resistance (D) in the indicated mice. (**E** and **F**) Concentrations of TGFβ (E) and IL-33 (F) in the lungs of the indicated mice exposed to normal ventilation alone (4 hours) or high stretch for 1 hour followed by 3 hours of normal ventilation. Statistical analysis was performed by repeated measured ANOVA (A to D) or by one-way ANOVA with Dunn-Šidák corrected post-hoc comparisons (E and F). ****$P < 0.0001$. Data are means ± SEM (A to D) or calculated mean values (E and F) from four to nine mice/group.

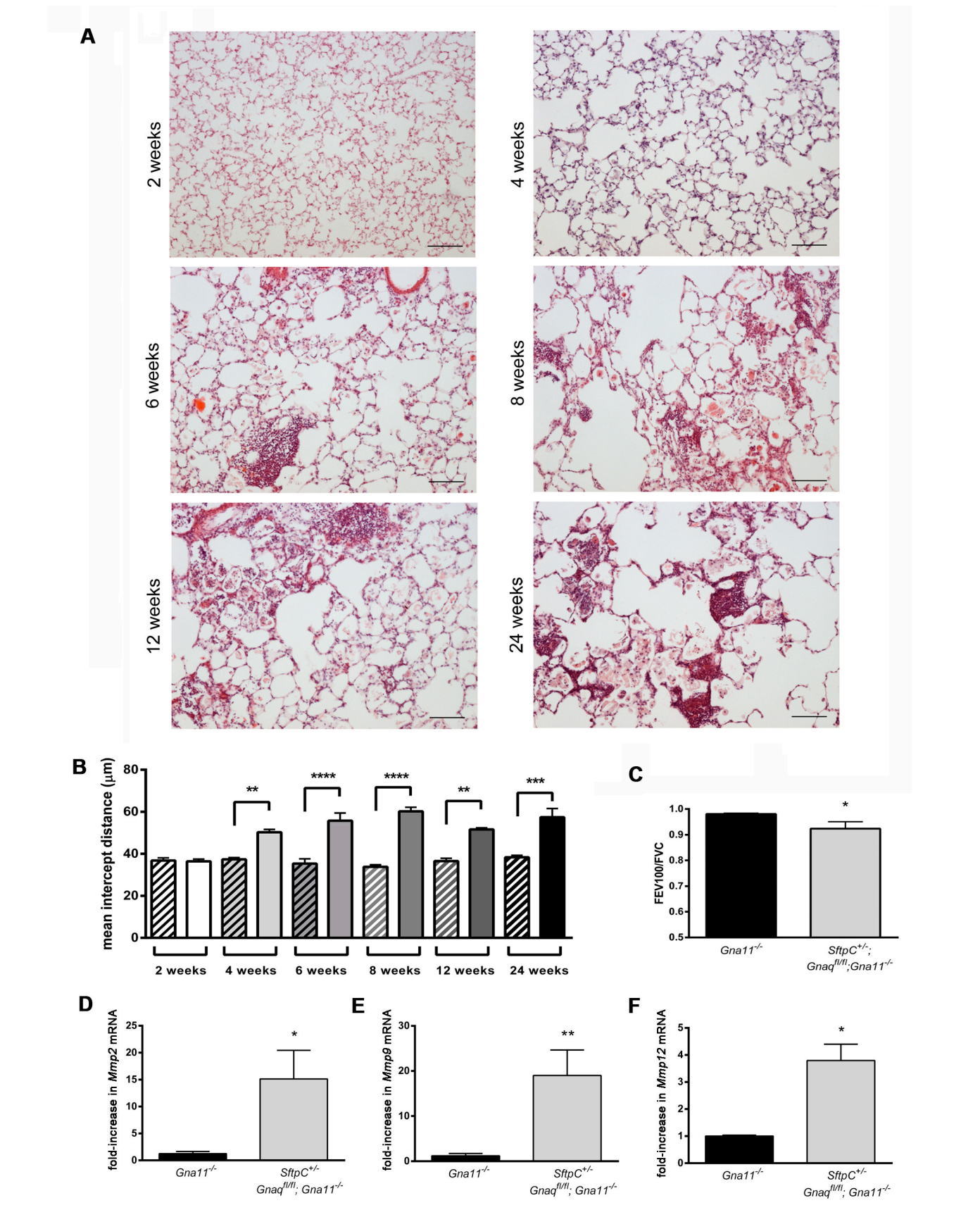
A
2 weeks
4 weeks
6 weeks
8 weeks
12 weeks
24 weeks
B
mean intercept distance (µm)
0
20
40
60
80
**
****
****
**
***
2 weeks
4 weeks
6 weeks
8 weeks
12 weeks
24 weeks
C
FEV100/FVC
0.5
0.6
0.7
0.8
0.9
1.0
*
Gna11-/-
SftpC+/-; Gnaqfl/fl;Gna11-/-
D
fold-increase in Mmp2 mRNA
0
5
10
15
20
25
*
Gna11-/-
SftpC+/- Gnaqfl/fl; Gna11-/-
E
fold-increase in Mmp9 mRNA
0
10
20
30
**
Gna11-/-
SftpC+/- Gnaqfl/fl; Gna11-/-
F
fold-increase in Mmp12 mRNA
0
1
2
3
4
5
*
Gna11-/-
SftpC+/- Gnaqfl/fl; Gna11-/-

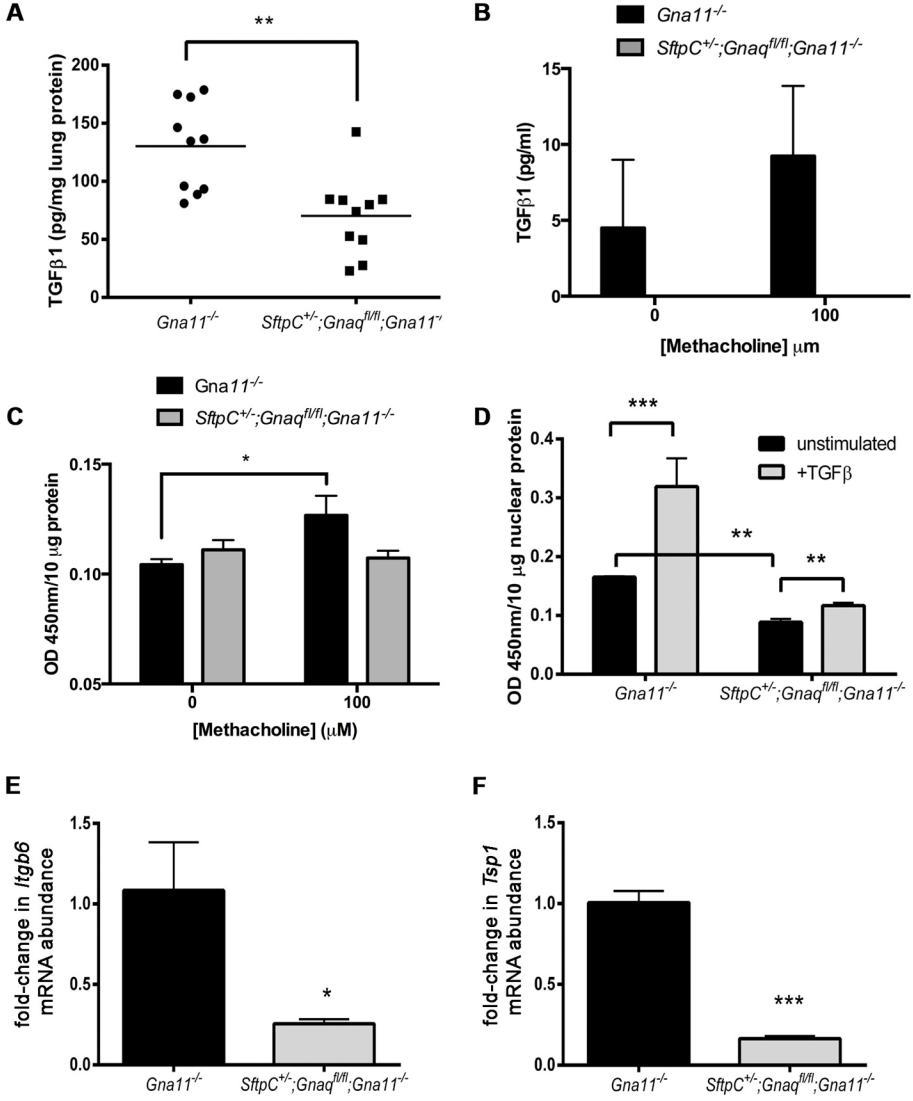
A
**
TGFβ1 (pg/mg lung protein)
200
150
100
50
0
Gna11-/-
SftpC+/-;Gnaqfl/fl;Gna11-/-
B
Gna11-/-
SftpC+/-;Gnaqfl/fl;Gna11-/-
TGFβ1 (pg/ml)
15
10
5
0
0
100
[Methacholine] μm
C
Gna11-/-
SftpC+/-;Gnaqfl/fl;Gna11-/-
*
OD 450nm/10 μg protein
0.15
0.10
0.05
0
100
[Methacholine] (μM)
D
***
**
**
unstimulated
+TGFβ
OD 450nm/10 μg nuclear protein
0.4
0.3
0.2
0.1
0.0
Gna11-/-
SftpC+/-;Gnaqfl/fl;Gna11-/-
E
fold-change in Itgb6 mRNA abundance
1.5
1.0
0.5
0.0
*
Gna11-/-
SftpC+/-;Gnaqfl/fl;Gna11-/-
F
fold-change in Tsp1 mRNA abundance
1.5
1.0
0.5
0.0
***
Gna11-/-
SftpC+/-;Gnaqfl/fl;Gna11-/-

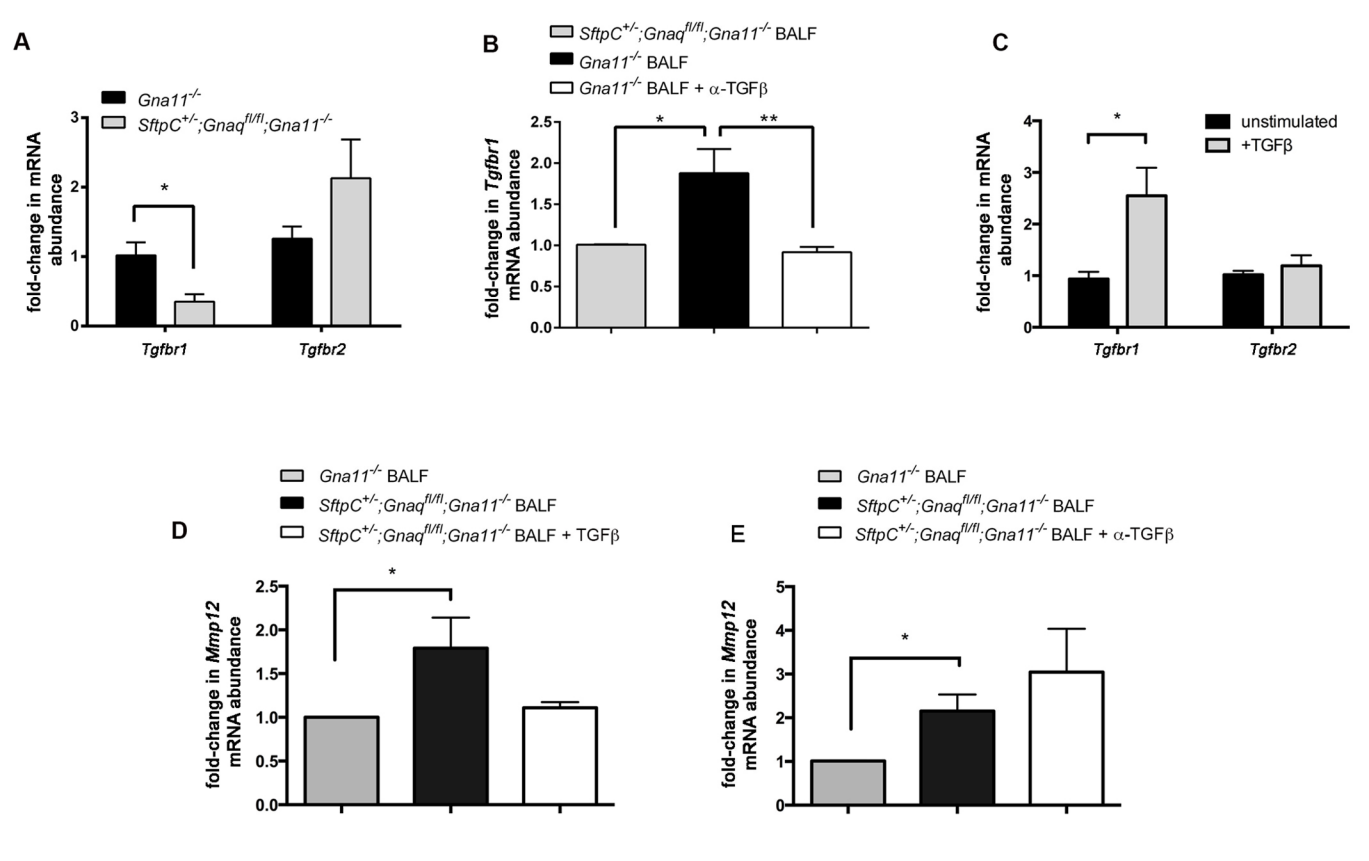
A
Gna11-/-
SftpC+/-;Gnaqfl/fl;Gna11-/-
fold-change in mRNA abundance
Tgfbr1
Tgfbr2
B
SftpC+/-;Gnaqfl/fl;Gna11-/- BALF
Gna11-/- BALF
Gna11-/- BALF + α-TGFβ
fold-change in Tgfbr1 mRNA abundance
C
unstimulated
+TGFβ
fold-change in mRNA abundance
Tgfbr1
Tgfbr2
D
Gna11-/- BALF
SftpC+/-;Gnaqfl/fl;Gna11-/- BALF
SftpC+/-;Gnaqfl/fl;Gna11-/- BALF + TGFβ
fold-change in Mmp12 mRNA abundance
E
Gna11-/- BALF
SftpC+/-;Gnaqfl/fl;Gna11-/- BALF
SftpC+/-;Gnaqfl/fl;Gna11-/- BALF + α-TGFβ
fold-change in Mmp12 mRNA abundance

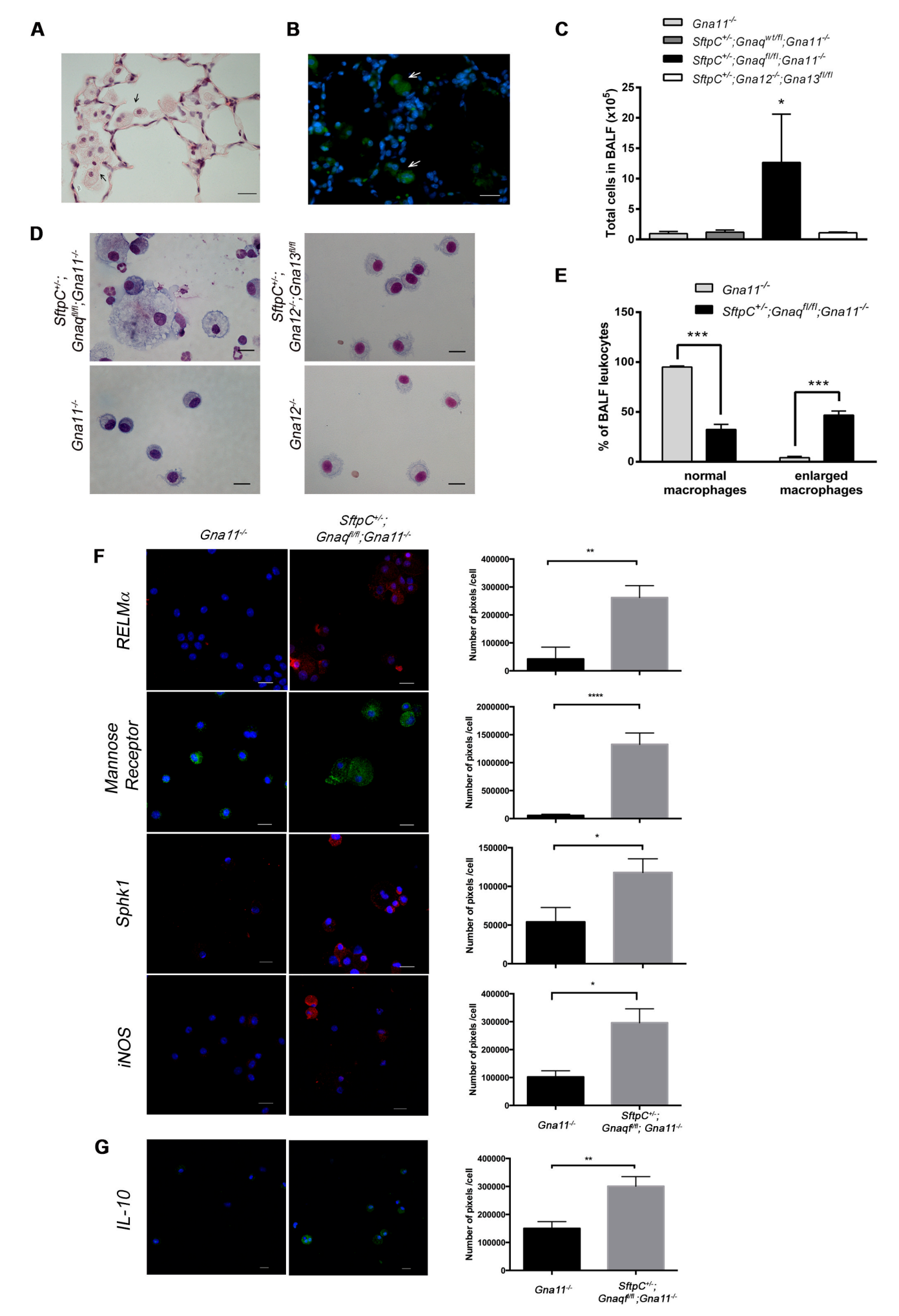
A
B
C
Gna11-/-
SftpC+/-;Gnaqwt/fl;Gna11-/-
SftpC+/-;Gnaqfl/fl;Gna11-/-
SftpC+/-;Gna12-/-;Gna13fl/fl
Total cells in BALF (x10^5)
25
20
15
10
5
0
*
D
SftpC+/-; Gnaqfl/fl;Gna11-/-
Gna11-/-
SftpC+/-; Gna12-/-;Gna13fl/fl
Gna12-/-
E
Gna11-/-
SftpC+/-;Gnaqfl/fl;Gna11-/-
% of BALF leukocytes
150
100
50
0
***
***
normal macrophages
enlarged macrophages
F
Gna11-/-
SftpC+/-; Gnaqfl/fl;Gna11-/-
RELMα
Mannose Receptor
Sphk1
iNOS
Number of pixels /cell
400000
300000
200000
100000
0
**
2000000
1500000
1000000
500000
****
150000
100000
50000
*
Gna11-/-
SftpC+/-; Gnaqfl/fl; Gna11-/-
G
IL-10
Gna11-/-
SftpC+/-; Gnaqfl/fl;Gna11-/-

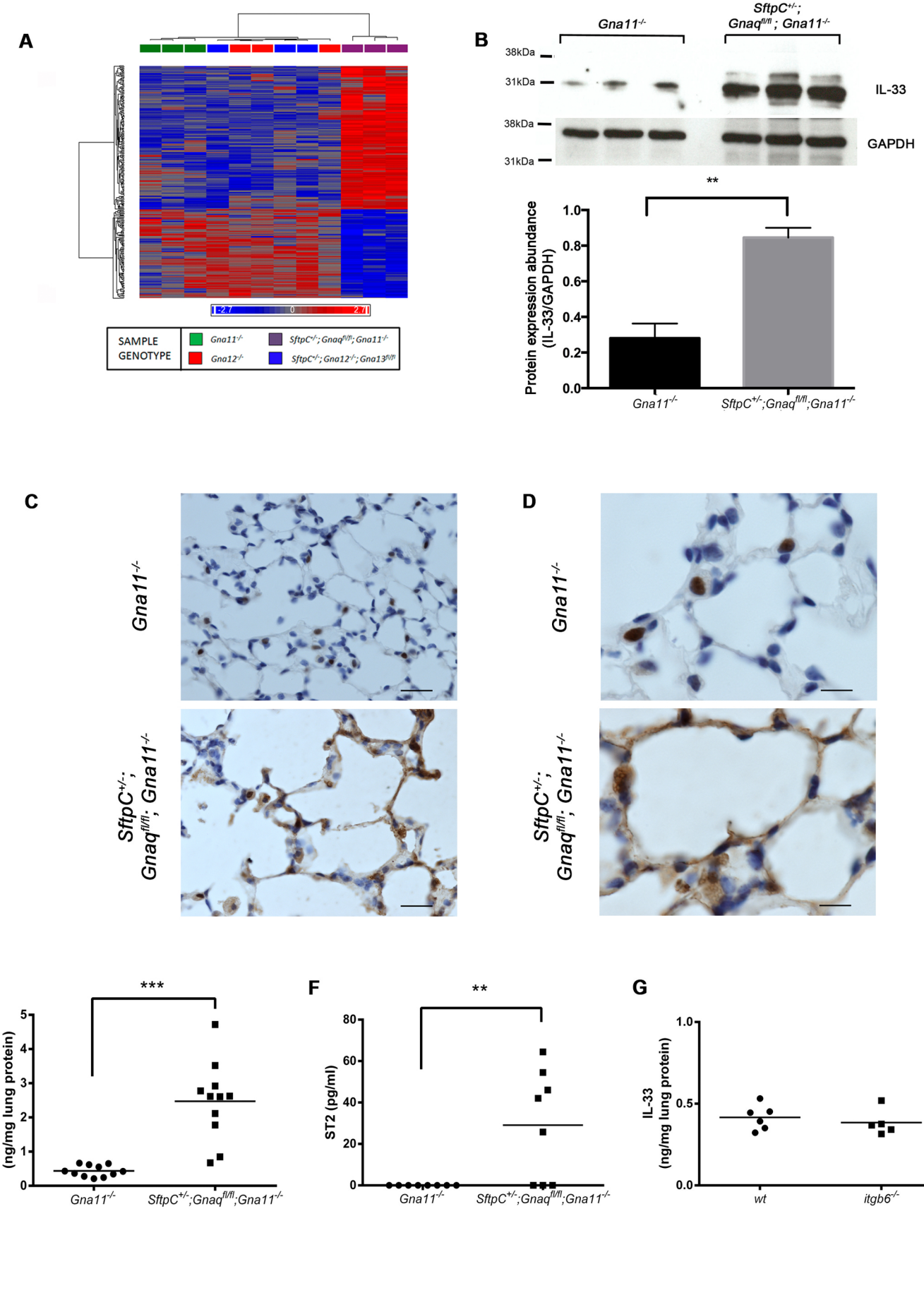
A
SAMPLE GENOTYPE
Gna11-/-
Gna12-/-
SftpC+/-;Gnaqfl/fl;Gna11-/-
SftpC+/-;Gna12-/-;Gna13fl/fl
B
Gna11-/-
SftpC+/-; Gnaqfl/fl ; Gna11-/-
38kDa
31kDa
38kDa
31kDa
IL-33
GAPDH
**
Protein expression abundance (IL-33/GAPDH)
1.0
0.8
0.6
0.4
0.2
0.0
Gna11-/-
SftpC+/-;Gnaqfl/fl;Gna11-/-
C
Gna11-/-
SftpC+/-; Gnaqfl/fl; Gna11-/-
D
Gna11-/-
SftpC+/-; Gnaqfl/fl; Gna11-/-
E
***
IL-33 (ng/mg lung protein)
5
4
3
2
1
0
Gna11-/-
SftpC+/-;Gnaqfl/fl;Gna11-/-
F
**
ST2 (pg/ml)
80
60
40
20
0
Gna11-/-
SftpC+/-;Gnaqfl/fl;Gna11-/-
G
IL-33 (ng/mg lung protein)
1.0
0.5
0.0
wt
itgb6-/-

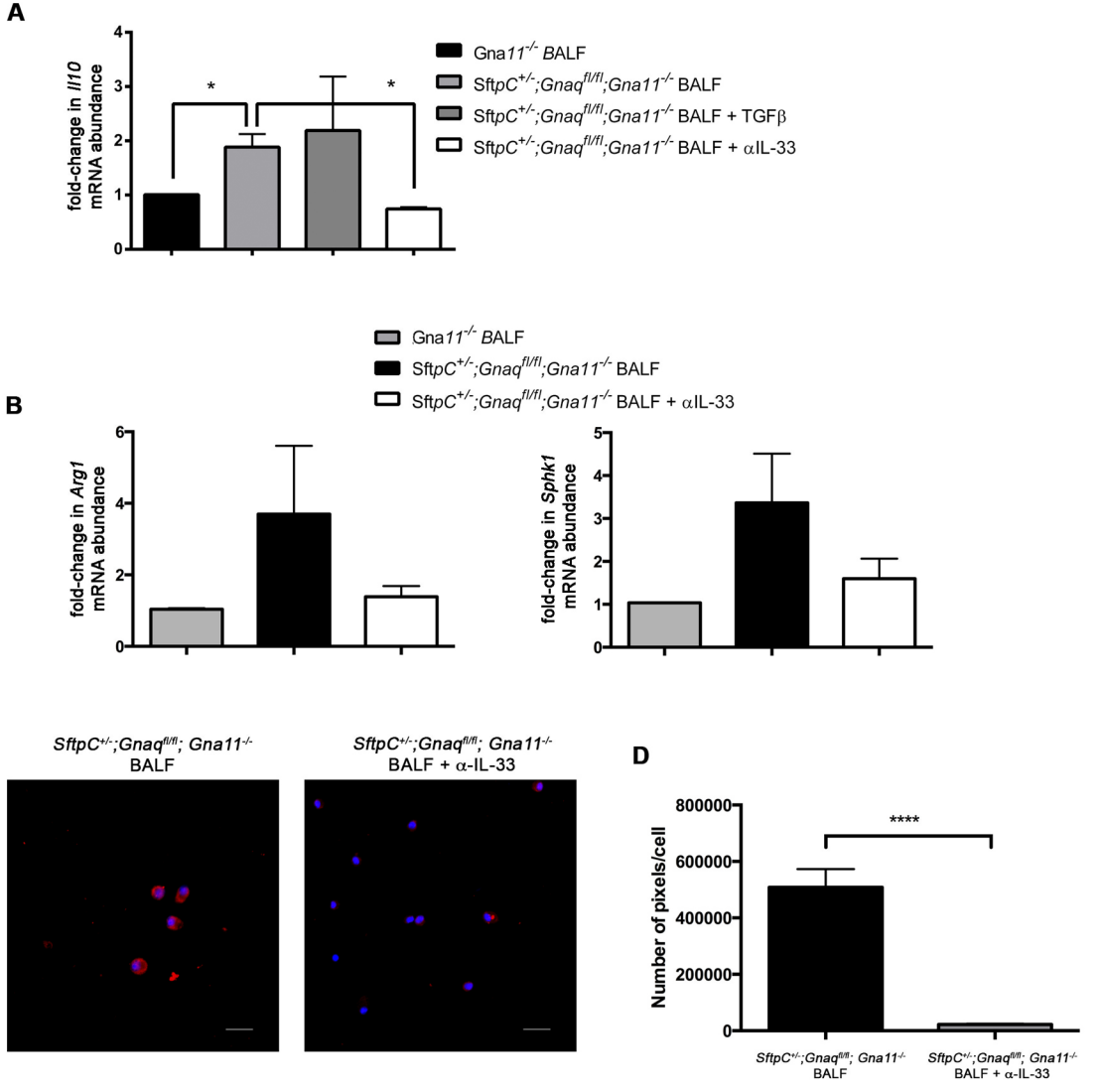
A
fold-change in Il10 mRNA abundance
Gna11-/- BALF
SftpC+/-;Gnaqfl/fl;Gna11-/- BALF
SftpC+/-;Gnaqfl/fl;Gna11-/- BALF + TGFβ
SftpC+/-;Gnaqfl/fl;Gna11-/- BALF + αIL-33
B
Gna11-/- BALF
SftpC+/-;Gnaqfl/fl;Gna11-/- BALF
SftpC+/-;Gnaqfl/fl;Gna11-/- BALF + αIL-33
fold-change in Arg1 mRNA abundance
fold-change in Sphk1 mRNA abundance
C
SftpC+/-;Gnaqfl/fl; Gna11-/- BALF
SftpC+/-;Gnaqfl/fl; Gna11-/- BALF + α-IL-33
D
Number of pixels/cell
****
SftpC+/-;Gnaqfl/fl; Gna11-/- BALF
SftpC+/-;Gnaqfl/fl; Gna11-/- BALF + α-IL-33

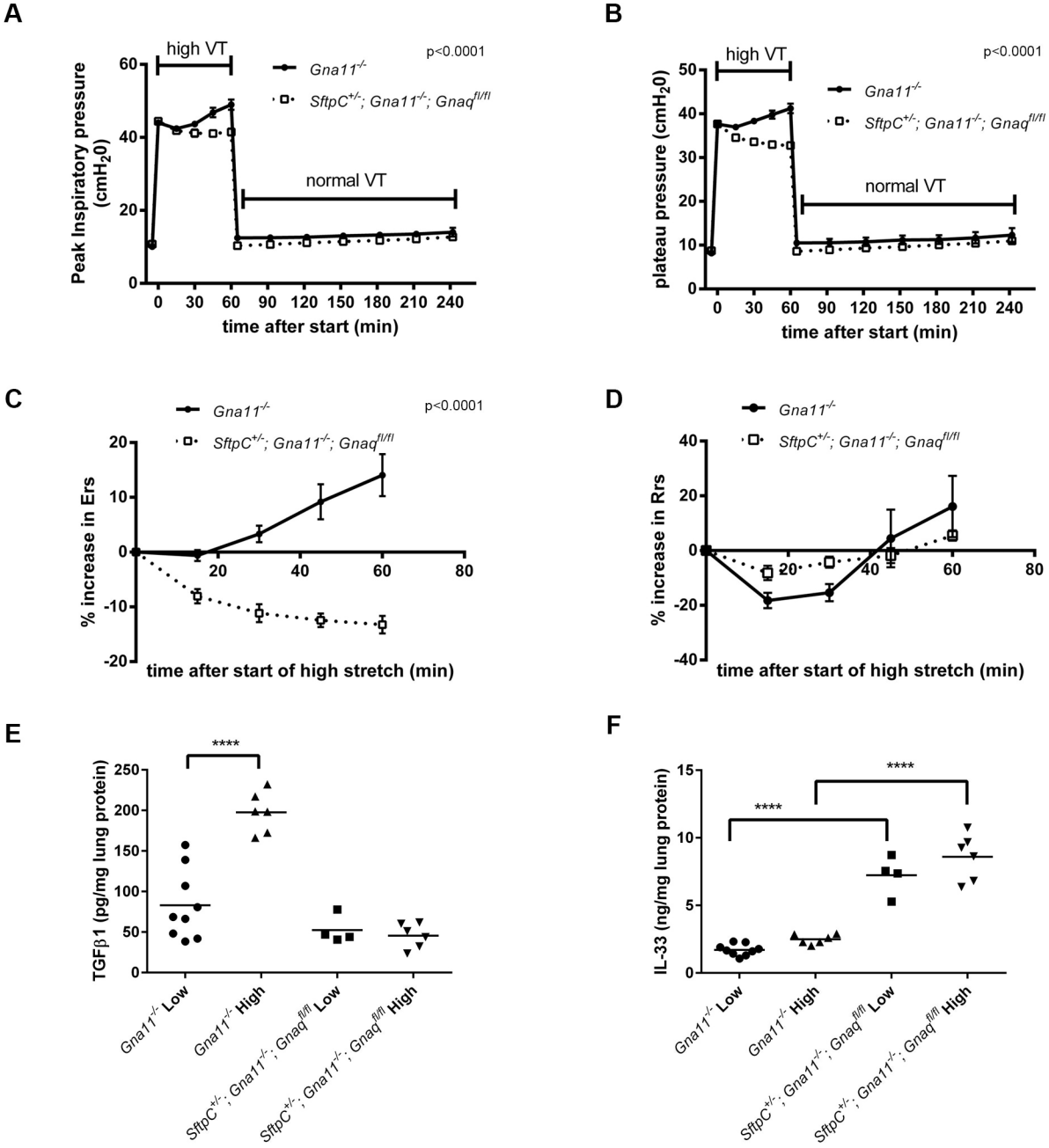
A
high VT
normal VT
p<0.0001
Gna11-/-
SftpC+/-; Gna11-/-; Gnaqfl/fl
Peak Inspiratory pressure (cmH20)
time after start (min)
B
high VT
normal VT
p<0.0001
Gna11-/-
SftpC+/-; Gna11-/-; Gnaqfl/fl
plateau pressure (cmH20)
time after start (min)
C
p<0.0001
Gna11-/-
SftpC+/-; Gna11-/-; Gnaqfl/fl
% increase in Ers
time after start of high stretch (min)
D
Gna11-/-
SftpC+/-; Gna11-/-; Gnaqfl/fl
% increase in Rrs
time after start of high stretch (min)
E
****
TGFβ1 (pg/mg lung protein)
Gna11-/- Low
Gna11-/- High
SftpC+/-; Gna11-/-; Gnaqfl/fl Low
SftpC+/-; Gna11-/-; Gnaqfl/fl High
F
****
****
IL-33 (ng/mg lung protein)
Gna11-/- Low
Gna11-/- High
SftpC+/-; Gna11-/-; Gnaqfl/fl Low
SftpC+/-; Gna11-/-; Gnaqfl/fl High